Hindawi
Journal of Chemistry
Volume 2022, Article ID 2336175, 17 pages
https://doi.org/10.1155/2022/2336175

Research Article

3,5-Dinitrobenzoate and 3,5-Dinitrobenzamide Derivatives: Mechanistic, Antifungal, and *In Silico* Studies

Allana B. S. Duarte,[1] **Yunierkis Perez-Castillo**,[2] **Patrícia Néris Andrade**,[3] **Ricardo D. de Castro**,[3] **and Damião P. de Sousa**[1,4]

[1]*Postgraduate Program in Natural and Synthetic Bioactive Products, Federal University of Paraíba, João Pessoa, PB, Brazil*
[2]*Facultad de Ingeniería y Ciencias Aplicadas, Área de Ciencias Aplicadas, Universidad de Las Américas, Quito 170516, Ecuador*
[3]*Laboratory of Experimental Pharmacology and Cell Culture, Department of Clinical and Social Dentistry, Federal University of Paraíba, João Pessoa 58051-900, PB, Brazil*
[4]*Department of Pharmaceutical Sciences, Federal University of Paraíba, João Pessoa, PB, Brazil*

Correspondence should be addressed to Damião P. de Sousa; damiao_desousa@yahoo.com.br

Received 1 July 2022; Revised 18 August 2022; Accepted 21 August 2022; Published 19 September 2022

Academic Editor: Maria F. Carvalho

Fungal infections, including those caused by *Candida* spp., are recognized in immunocompromised individuals for their high rates of morbidity and mortality. Microorganism resistance to conventional drugs compromises treatment effectiveness and yet also reveals the need to develop new drugs. In many compounds, nitro groups contribute to antimicrobial activity; thus, the inhibitory activity of a collection of twenty esters and amides (derived from 3,5-dinitrobenzoic acid) against *Candida* spp. was elucidated using microdilution methods to determine the Minimum Inhibitory Concentration (MIC) and Minimum Fungicide Concentration (MFC), as well as probable mechanisms of action. The structures of the synthesized compounds were characterized by FTIR spectroscopy, ^{1}H-NMR, ^{13}C NMR, and HRMS. Of the tested derivatives, ten presented fungicidal activity against at least one of the tested strains. Ethyl 3,5-dinitrobenzoate (**2**) exhibited the most potent antifungal activity against *Candida albicans* (MIC = 125 μg/mL; 0.52 mM), *Candida krusei* (MIC = 100 μg/mL; 4.16 mM), and *Candida tropicalis* (MIC = 500 μg/ml; 2.08 mM). The structure of the second most potent derivative (propyl 3,5-dinitrobenzoate (**3**) reveals that esters with short alkyl side chains exhibit better biological activity profiles. Compounds **2** and **3** presented a mechanism of action involving the fungal cell membrane. Though compound **2** modeling against *C. albicans* revealed a multitarget antifungal mechanism of action, involving various cellular processes, interference in the synthesis of ergosterol was observed. Our results demonstrate that certain ester derivatives containing aromatic ring nitro groups may be useful in the search for new antifungal drugs.

1. Introduction

Fungal infections, due to their progressive increase and high rates of morbidity and mortality, have assumed great importance in recent years. Many such infections are acquired endogenously; others are acquired exogenously, coming from the hands of health professionals, instruments, and biomaterials. Of these infections, those caused by *Candida* yeast are the most frequent and depending on the affected site, in various manifestations, whether being superficial or invasive is associated with immunosuppression [1–3]. Azoles, allylamines, polyenes, and echinocandins are primary treatments for systemic fungal infections and superficial mycoses. However, these drug classes present a number of disadvantages in terms of toxicity, safety, and pharmacokinetics [4–6].

Resistance to antifungal therapy continues to increase and evolve, contributing to fungal disease and posing a serious threat to public health. Fungi, to counteract the fungicidal or fungistatic effects of drugs, develop many resistance mechanisms and are based on either lowering the effective concentration of the drug, altering the drug target

itself, or on modifying their own metabolism to deflect the toxic effects exerted by the drug [6–8]. Further, if compared to the development of new antibacterial drugs, antifungal drugs present more difficulties because fungi are eukaryotic microorganisms, and many therapy targets are shared by humans, increasing the risk of toxicity [6, 9].

Benzoic acid and its derivatives when substituted are extremely important in medicine and in the chemical and pharmaceutical industries. 3,5-Dinitrobenzoic acid is an important intermediate for the pharmaceutical industry and presents electron-withdrawing nitro groups. Nitro groups are present in the structures of many bioactive substances and possess various pharmacological activities [10–13]. Inside the cells of parasites, bacteria, and fungi, $-NO_2$ (a strong electron acceptor) presents electron-withdrawing character, with a reducing capacity that results in the formation of free radicals causing damage by oxidative stress through interactions with biomolecules that are essential to microorganism survival [14]. Previous studies by Nascimento [15] and Ferreira [16] have shown that certain nitro-compounds derived from *o*-nitrocinnamic acid and 3-methyl-4-nitrobenzoic acid present antifungal activity against strains of the *Candida* genus [15, 16]. The aim of the present study was to prepare a series of esters and amides derived from 3,5-dinitrobenzoic acid and to evaluate their antifungal activity against strains of the genus *Candida*.

2. Materials and Methods

2.1. Chemistry

2.1.1. Materials. All reagents necessary for chemical synthesis were obtained from Sigma-Aldrich. Adsorption column chromatography (CC) was performed using silica gel 60, ART 7734 from MERCK as the stationary phase (particle sizes between 0.063 and 0.200 mm). TLC was obtained using silica gel sheet chromatographs (Merck 60 F 254). The ^{1}H NMR and ^{13}C NMR spectra were recorded in Bruker Avance III HD spectrometers operating at 400 MHz (^{1}H) and 100 MHz (^{13}C), and with a Varian NMR operating at 500 MHz (^{1}H) and 125 MHz (^{13}C). Chemical shifts were expressed in parts per million (ppm), and the multiplicities of the ^{1}H NMR bands were indicated according to the conventions: *s* (singlet), *d* (doublet), *t* (triplet), *quint* (quintet), *sext* (sext), *sept* (septet), and *m* (multiplet). FTIR spectra were obtained using an Agilent technologies Cary 630 FTIR instrument, in the 4000–400 cm^{-1} spectral range. The high-resolution mass spectrum was performed at the Centro de Tecnologias Estratégicas do Nordeste (CETENE), in an Ultraflex II TOF/TOF equipment with a high-performance solid-state laser ($\lambda = 355$ nm) and a reflector, using the MALDI technique—Matrix Assisted Laser Desorption Ionization. The sample was loaded onto a steel plate (MTP 384 steel base; Bruker Daltonics GmbH, Bremen, Germany). Spectroscopic data for the compounds in this study are available in the Supplementary Materials.

*2.1.2. General Procedure: Preparation of Compounds **2–7**.* 3,5-Dinitrobenzoic acid (0.100 g, 0.47 mmol) was dissolved in 20 mL of ROH. Subsequently, 0.025 ml of sulfuric acid H_2SO_4 (96% v/v) was added. The reaction mixture was stirred and heated under reflux for 3–24 hours and monitored by TLC. After completion of the reaction, the solvent was partially removed under reduced pressure, and the solution was diluted in 20 ml of water. The product obtained was extracted with ethyl acetate (3×15 ml), and the organic phase was treated successively with a 5% $NaHCO_3$ solution, water, dried with Na_2SO_4, filtered, and roto-evaporated yielding the ester derivative. The products were purified using silica gel 60 column chromatography and hexane and ethyl acetate as eluents in an increasing polarity gradient [17].

*2.1.3. General Procedure: Obtaining Derivatives **8** and **9**.* 3,5-Dinitrobenzoic acid (0.1 g, 0.47 mmol) was dissolved in 15 mL of acetone. Subsequently, 0.25 mL of triethylamine (1.89 mmol) and the halide (0.49 mmol) were added. The reaction mixture was heated under reflux for 48 hours and monitored by TLC. The solvent was then partially evaporated under reduced pressure. The product obtained was extracted with ethyl acetate (3×20 ml), and the organic phase was washed successively with distilled water, dried over Na_2SO_4, filtered, and evaporated under reduced pressure. The residues were purified using a silica gel 60 chromatography column, and a mixture of hexane and ethyl acetate (eluent) in an increasing polarity gradient [18, 19].

*2.1.4. General Procedure: Obtaining Derivatives **10–12**.* 3,5-Dinitrobenzoic acid (0.1 g, 0.47 mmol) and alcohol (0.47 mmol) were dissolved in 1.57 mL of tetrahydrofuran (THF). The contents were kept under magnetic stirring at 0°C for 30 minutes. Esterification agents di-isopropyl azodicarboxylate (0.09 mL; 0.47 mmol) and triphenylphosphine—PPh_3 (0.12 g; 0.47 mmol) were then added, and stirring was continued at room temperature for 72 hours, being monitored by TLC. To start the extraction, the solvent was partially roto-evaporated under reduced pressure. The product obtained was extracted with ethyl acetate (3×10 ml), and the organic phase was then neutralized with 5% $NaHCO_3$ washed with distilled water and dried with anhydrous Na_2SO_4 and filtered, and the solvent removed under reduced pressure. The residues were purified using silica gel 60 column chromatography, with a mixture of hexane and ethyl acetate in differing proportions as eluent [20].

*2.1.5. General Procedure: Synthesis of Derivatives **13–14**.* 3,5-Dinitrobenzoic acid (0.1 g, 0.47 mmol) was reacted with 3.17 mL of $SOCl_2$ (43.51 mmol) under reflux for 3 hours. Upon completion, the excess $SOCl_2$ was removed under reduced pressure. The acid chloride formed was dissolved in

CH_2Cl_2 (1 mL) and used without further purification. In another flask, 0.08 g (0.57 mmol) of alcohol dissolved in 4 mL of CH_2Cl_2 was added. An acid chloride solution (1 mL) was added dropwise to the solution at 0°C. The resulting mixture was kept at room temperature and stirred for 1 hour. The reaction was monitored by TLC. The products were purified using silica gel 60 column chromatography with hexane and ethyl acetate as eluents in an increasing polarity gradient [21].

*2.1.6. General Procedure: Synthesis of Derivatives **15**–**21**.* 3,5-Dinitrobenzoic acid (0.1 g, 0.47 mmol) was reacted with 3.17 mL of $SOCl_2$ (43.51 mmol) under reflux for 3 hours. After the reaction, excess $SOCl_2$ was removed with the aid of a rotary evaporator. The acid chloride formed was dissolved in dichloromethane (1 mL) and added dropwise to a solution of the amine (0.57 mmol, 1.2 eq.) in CH_2Cl_2 (4 mL) and Et_3N (0.07 g, 0.70 mmol) at 0°C. The resulting mixture was kept at room temperature and magnetically stirred for 1 hour, monitored by TLC. The products were purified using silica gel 60 column chromatography with hexane and ethyl acetate as eluents in an increasing polarity gradient [21].

*Ethyl 3,5-dinitrobenzoate (**2**)* amber amorphous solid; 81.61% yield; TLC (9:1hexane/EtOAc); $R_f = 0.39$; m.p.: 90.1–90.5°C (lit. 92–93°C [22]); IR υmax (KBr, cm^{-1}): 3093, 2984, 1731, 1627 and 1467, 1544 and 1347, 1277 and 1180; ^{1}H NMR (400 MHz, $CDCl_3$): δ_H 9.21 (*t*; $J = 2.1$ Hz; 1H), 9.15 (*d*; $J = 2.1$ Hz; 2H), 4.52 (*q*; $J = 7.2$ Hz; 2H); 1.47 (*t*; $J = 7.2$ Hz; 3H); ^{13}C NMR (101 MHz, $CDCl_3$): δ_C: 162.62, 148.78, 134.27, 129.55, 122.42, 63.14, 14.35 [22].

*Propyl 3,5-dinitrobenzoate (**3**)* amber amorphous solid; 78.02% yield; TLC (9:1hexane/EtOAc); $R_f = 0.48$; m.p.: 69.8–70.4°C (lit. 72.8–73.8°C, [23]); IR υmax (KBr, cm^{-1}): 3114, 2969, 1723, 1633 and 1461, 1546 and 1347, 1295 and 1117; ^{1}H NMR (400 MHz, $CDCl_3$): δ_H 9.23 (*t*; $J = 2.2$ Hz; 1H), 9.17 (*d*; $J = 2.2$ Hz; 2H), 4.43 (*t*; $J = 6.8$ Hz; 2H), 1.92–1.83 (*sext*; $J = 7.5$ Hz; 2H), 1.07 (*t*; $J = 7.4$ Hz; 3H); ^{13}C NMR (100 MHz, $CDCl_3$): δ_C 162.69, 148.81, 134.30, 129.54, 122.40, 68.62, 22.10, 10.52 [24].

*Isopropyl 3,5-dinitrobenzoate (**4**)* amber amorphous solid; 82.36% yield; TLC (9:1hexane/EtOAc); $R_f = 0.51$; m.p.: 114.5–114.8°C (lit. 118–119°C, [25]); IR υmax (KBr, cm^{-1}): 3118, 2989, 1718, 1631 and 1461, 1548 and 1347, 1292 and 1178; ^{1}H NMR (400 MHz, $CDCl_3$): δ_H 9.21 (*t*; $J = 2.2$ Hz; 1H), 9.15 (*d*; $J = 2.2$ Hz; 2H), 5.38(*sept*; $J = 6.3$ Hz; 1H), 1.46 (*d*; $J = 6.3$ Hz; 6H); ^{13}C NMR (100 MHz, $CDCl_3$): δ_C 162.10, 148.76, 134.70, 129.52, 122.31, 71.31, 21.95 [24].

*Butyl 3,5-dinitrobenzoate (**5**)* amber crystal solid; 78.53% yield; TLC (9:1hexane/EtOAc); $R_f = 0.55$; m.p.: 62.7–63.1°C (lit. 63°C [26]); IR υmax (KBr, cm^{-1}): 3113, 2963, 1721, 1631 and 1465, 1548 and 1346, 1286 and 1176; ^{1}H NMR (400 MHz, $CDCl_3$): δ_H 9.21 (*t*; $J = 2.2$ Hz; 1H), 9.15 (*d*; $J = 2.1$ Hz; 2H), 4.46 (*t*; $J = 6.7$ Hz; 2H), 1.82 (*quint*; $J = 6.7$ Hz; 2H), 1.50 (*sext*; $J = 7.5$ Hz; 2H), 1.01 (*t*; $J = 7.4$ Hz; 3H); ^{13}C NMR (100 MHz, $CDCl_3$): δ_C 162.69, 148.80, 134.30, 129.53, 122.41, 66.97, 30.66,19.23, 13.82 [26].

*Pentyl 3,5-dinitrobenzoate (**6**)* brown amorphous solid; 72.52% yield; TLC (9:1hexane/EtOAc); $R_f = 0.69$; m.p.: 43.7–43.8°C (lit. 46.4°C [27]); IR υmax (KBr, cm^{-1}): 3097, 2962, 1729, 1629 and 1461, 1543 and 1346, 1286 and 1172; ^{1}H NMR (400 MHz, $CDCl_3$): δ_H 9.21 (*t*; $J = 2.2$ Hz; 1H), 9.15 (*d*; $J = 2.2$ Hz; 2H), 4.44 (*t*; $J = 6.8$ Hz; 2H); 1.83 (*quint*; $J = 7.0$ Hz; 2H); 1.45–1.39 (*m*; 4H), 0.94 (*t*; $J = 7.1$ Hz; 3H); ^{13}C NMR (100 MHz, $CDCl_3$): δ_C 162.71, 148.82, 134.32, 129.55, 122.43, 67.29, 28.39, 28.15, 22.43, 14.06 [28].

*Isopentyl 3,5-dinitrobenzoate (**7**)* yellow crystal solid; 68.84% yield; TLC (9:1hexane/EtOAc)); $R_f = 0.74$; m.p.: 59.9–60.2°C (lit. 61–62°C [29]); IR υmax (KBr, cm^{-1}): 3111, 2964, 1721, 1631 and 1463, 1547 and 1348, 1293 and 1174; ^{1}H NMR (400 MHz, $CDCl_3$): δ_H 9.22 (*t*; $J = 2.2$ Hz; 1H), 9.15 (*d*; $J = 2.1$ Hz; 2H), 4.49 (*t*; $J = 6.8$ Hz; 2H), 1.83–1.70 (*m*; 3H), 1.00 (*d*; $J = 6.4$ Hz; 6H); ^{13}C NMR (100 MHz, $CDCl_3$): δ_C 162.769 148.78, 134.28, 129.54, 122.44, 65.82, 37.31, 25.28, 22.59 [30].

*Decyl 3,5-dinitrobenzoate (**8**)* yellow amorphous solid; 44.79% yield; TLC (9:1hexane/EtOAc); $R_f = 0.74$; m.p.: 53.2–53.7°C (lit. 44.6°C, [31]); IR υmax (KBr, cm^{-1}): 3095, 2922, 1728, 1627 and 1461, 1542 and 1346, 1288 and 1171; ^{1}H NMR (400 MHz, $CDCl_3$): δ_H 9.22 (*t*; $J = 2.2$ Hz; 1H), 9.15 (*d*; $J = 2.2$ Hz; 2H), 4.45 (*t*; $J = 6.8$ Hz; 2H), 1.83 (*quint*; $J = 6.8$ Hz; 2H), 1.46–1.27 (*m*; 14H), 0.87 (*t*; $J = 6.8$ Hz; 3H); ^{13}C NMR (100 MHz, $CDCl_3$): δ 162.70, 148.81, 134.33,129.54, 122.37, 67.30, 32.00, 29.64, 29.61, 29.42, 29.35, 28.68, 26.02, 22.80, 14.23 [31].

*4-Chlorobenzyl 3,5-dinitrobenzoate (**9**)* yellow crystal solid; Yield: 33.42%; Rf (9:1Hexane/EtOAc); $R_f = 0.41$; m.p.: 123.7–123.9°C; IR υmax (KBr, cm^{-1}): 3101, 2885, 1720, 1629 and 1493, 1545 and 1347, 1277 and 1167, 1014; ^{1}H NMR (400 MHz, $CDCl_3$): δ: 9.22 (*t*; $J = 2.2$ Hz; 1H), 9.15 (*d*; $J = 2.1$ Hz; 2H), 7.44–7.38 (*m*; 4H), 5.44 (*s*; 2H); ^{13}C NMR (100 MHz, $CDCl_3$) δ: 162.46, 148.83, 135.24, 133.76, 133.11, 130.42, 129.64, 129.25, 122.74, 67.90; HRMS (MALDI) calculated for $C_{14}H_9ClN_2O_6$ $[M+H]^+$: 337.023, found 337.026.

*Benzyl 3,5-dinitrobenzoate (**10**)* yellow amorphous solid; 23.86% yield; TLC (9:1hexane/EtOAc); $R_f = 0.48$; m.p.: 106.4–106.9°C (lit. 117–118°C, [32]); IR υmax (KBr, cm^{-1}): 3103, 2877, 1740, 1629 and 1498, 1540 and 1347, 1278 and 1168; ^{1}H NMR (400 MHz, $CDCl_3$): δ_H 9.21(*t*; $J = 2.2$ Hz; 1H), 9.17 (*d*; $J = 2.1$ Hz; 2H), 7.49–7.46 (*m*; 2H), 7.45–7.39 (*m*; 3H), 5.48 (*s*; 2H); ^{13}C NMR (100 MHz, $CDCl_3$): δ_C 162.54, 148.84, 134.67, 134.02, 129.64, 129.18, 129.02, 128.95, 122.57, 68.77 [30, 32, 33].

*4-Methoxy-benzyl 3,5-dinitrobenzoate (**11**)* yellow amorphous solid; 18.67% yield; TLC (9 : 1 hexane/EtOAc); R_f 0.39; m.p.: 89.2–89.6°C (lit. 101–102°C [34]); IR υmax (KBr, cm^{-1}): 3092, 2963, 1719 1629 and 1461, 1543 and 1348, 1282 and 1163; ^{1}H NMR (400 MHz, $CDCl_3$): δ_H 9.20 (*t*; $J = 2.1$ Hz; 1H), 9.15 (*d*; $J = 2.1$ Hz; 2H), 7.41 (*d*; $J = 8.8$ Hz; 2H), 6.93 (*d*; $J = 8.8$ Hz; 2H), 5.41 (*s*; 2H), 3.82 (*s*; 3H); ^{13}C NMR (100 MHz, $CDCl_3$): δ_C 162.58, 160.31, 148.73, 134.11, 130.92, 129.62, 126.55, 122.25, 114.32, 68.63, 55.46 [34].

*4-Isopropyl-benzyl 3,5-dinitrobenzoate (**12**)* white crystal solid; 48.05% yield; TLC (9 : 1 hexane/EtOAc); $R_f = 0.62$; m.p.: 92.8–93.2°C; IR υmax (KBr, cm^{-1}): 3076, 2962, 1729, 1627 and 1461, 1542 and 1349, 1275 and 1167; ^{1}H NMR (400 MHz, $CDCl_3$): δ_H 9.22 (*t*; $J = 2.2$ Hz; 1H), 9.17 (*d*;

$J = 2.1$ Hz; 2H), 7.41 (*d*; $J = 8.2$ Hz; 2H), 7.29 (*d*; $J = 8.0$ Hz; 2H), 5.44 (*s*; 2H), 2.94 (*sept*; $J = 6.8$ Hz; 1H), 1.27 (*d*; $J = 6.9$ Hz; 6H); ^{13}C NMR (100 MHz, $CDCl_3$): δ_C 162.59, 150.16, 148.78, 134.11, 131.98, 129.68, 129.23, 127.10, 122.55, 68.76, 34.10, 24.06 [35].

4-Nitro-benzyl 3,5-dinitrobenzoate (***13***) yellow crystal solid; 12.46% yield; TLC (9 : 1 hexane/EtOAc)); $R_f = 0.30$; m.p. 151.8–152.4°C; IR υmax (KBr, cm^{-1}): 3097, 2921, 1722, 1627 and 1452, 1543 and 1349, 1275 and 1160); ^{1}H NMR (500 MHz, DMSO-d6): δ_H 9.06 (*t*; $J = 2.1$ Hz; 1H), 8.96 (*d*; $J = 2.1$ Hz; 2H), 8.28 (*d*; $J = 8.8$ Hz; 2H), 7.81 (*d*; $J = 8.8$ Hz; 2H), 5.61 (*s*; 2H); ^{13}C NMR (125 MHz, DMSO-d6): δ_C 162.45, 148.45, 147.43, 142.96, 132.30, 129.09, 129.05, 123.72, 122.79, 66.51 [33].

3-Methoxy-benzyl 3,5-dinitrobenzoate (***14***) yellow crystal solid; 25.60% yield; TLC (9 : 1 hexane/EtOAc); $R_f = 0.42$; m.p.: 123.1–123.3°C (lit. 124°C [36]); IR υmax (KBr, cm^{-1}): 3090 2963, 1728, 1631 and 1457, 1545 and 1349, 1282 and 1159; ^{1}H NMR (400 MHz, $CDCl_3$): δ_H 9.22 (*t*; $J = 2.1$ Hz; 1H), 9.17 (*d*; $J = 2.1$ Hz; 2H), 7.34 (*t*; $J = 7.9$ Hz; 1H), 7.04 (*d*; $J = 7.6$ Hz; 1H), 7.00–6.99 (*m*; 1H), 6.93 (*dd*; $J = 8.1$ Hz; $J = 2.2$ Hz; 1H), 5.44 (*s*; 2H), 3.84 (*s;* 3H); ^{13}C NMR (101 MHz, $CDCl_3$): δ_C 162.52, 160.04, 148.81, 136.10, 133.97, 130.12, 129.66, 122.59, 121.06, 114.56, 114.46, 68.60, 55.46 [33].

N-Benzyl-3,5-dinitrobenzamide (***15***) amber crystal solid; 47.17% yield; TLC (7 : 3 hexane/EtOAc); $R_f = 0{,}57$; m.p: 198.8–199.1°C, (lit. 202–203°C [37]); IR υmax (KBr, cm^{-1}): 3316, 3093, 2931, 1639, 1543 and 1343; ^{1}H NMR (400 MHz, DMSO-d6): δ_H 9.76 (*t*; $J = 5.7$ Hz; 1H), 9.11 (*d*; $J = 2.1$ Hz; 2H), 8.96 (*t*; $J = 2.1$ Hz; 1H), 7.36–7.33 (*m*; 5H), 4,56 (*d*; $J = 5{,}8$ Hz; 2H); ^{13}C RMN (100 MHz, DMSO-d6): δ_C 162.19, 148.27, 138.75, 136.80, 128.45, 127.65, 127.58, 127.12, 120.96, 43.21 [37].

N,N-Diethyl-3,5-dinitrobenzamide (***16***) amber crystal solid; 62.07% yield; TLC (7 : 3 hexane/EtOAc); $R_f = 0.42$; m.p.: 88.6–88.8°C (lit. 89–90°C, [38]); IR υmax (KBr, cm^{-1}): 3089, 2970, 1641, 1592, 1546 and 1343; ^{1}H NMR (500 MHz, $CDCl_3$): δ_H 9.05(*s*; 1H), 8.56 (*s*; 2H) 3.59 (*s*; 2H), 3.27(*s*; 2H), 1.29 (*s*; 3H), 1.20 (*s*; 3H); ^{13}C NMR (125 MHz, $CDCl_3$): δ_C 166.26, 148.63, 140.51, 126.96, 119.37, 43.779, 40.22, 14.38, 12.88 [39].

3,5-Dinitro-N-phenylbenzamide (***17***) amber crystal solid; 59.08% yield; TLC (7 : 3 hexane/EtOAc); $R_f = 0.64$; m.p.: 233.1–233.6°C (lit. 226°C, [40]); IR υmax (KBr, cm^{-1}): 3284, 3105, 1659, 1545 and 1334; ^{1}H NMR (500 MHz, DMSO-d6): δ_H 10.83 (*s*; 1H), 9.17 (*d*; $J = 2.1$ Hz; 2H), 9.00 (*t*; $J = 2.1$ Hz; 1H), 7.78 (*d*; $J = 7.6$ Hz; 2H), 7.41 (*t*; $J = 7.6$ Hz; 2H), 7.17 (*t*; $J = 7.4$ Hz; 1H); ^{13}C NMR (125 MHz, DMSO-d6): δ_C 161.24, 148.11, 138.25, 137.43, 128.75, 127.99, 124.54, 121.06, 120.72 [40].

N-(4-Chlorobenzyl)-3,5-dinitrobenzamide (***18***) amber crystal solid; 46.12% yield; TLC (7 : 3 hexane/EtOAc); $R_f = 0.48$; m.p.: 190.4–190.7°C; IR υmax (KBr, cm^{-1}): 3303, 3099, 2926 1644, 1535 and 1344; ^{1}H NMR (400 MHz, DMSO-d6): δ_H 9.77 (*t*; $J = 5.8$ Hz; 1H), 9.09 (*d*; $J = 2.1$ Hz; 2H), 8.96 (*t*; $J = 2.1$ Hz; 1H), 7.42–7.37 (*m*; 4H), 4.54 (*d*; $J = 5.8$ Hz; 2H); ^{13}C NMR (100 MHz, DMSO-d6): δ_C 162.24, 148.26, 137.81, 136.68, 131.70, 129.47, 128.38, 127.63, 121.00, 42.56 [41].

N-(4-Fluorobenzyl)-3,5-dinitrobenzamide (***19***) amber amorphous solid; 63.38% yield; TLC (7 : 3 hexane/EtOAc); $R_f = 0.48$; m.p.: 197.3–198.0°C (lit. 204–206°C, [42]); IR υmax (KBr, cm^{-1}): 3302, 3099, 2939, 1642, 1534 and 1342; ^{1}H NMR (500 MHz, DMSO-d6): δ_H 9.72 (*t*; $J = 5.7$ Hz; 1H), 9.09 (*d*; $J = 2.1$ Hz; 2H), 8.96 (*t*; $J = 2.1$ Hz; 1H), 7.42–7.39(*m*; 2H); 7.17 (*t*; $J = 8.9$ Hz; 2H), 4.53 (*d;* $J = 5.8$ Hz; 2H); ^{19}F NMR(500 MHz, DMSO-d6): −115.76 (*s*; 1F); ^{13}C NMR (125 MHz, DMSO-d6): δ_C 162.19 (*d*, $J_{C\text{-}F} = 20$ Hz, C-4′-F), 160.34, 148.19, 136.73, 134.87, 129.61, 129.54, 127.55, 120.87, 115.16, 114.99, 42.48 [42].

N-Cyclohexyl-3,5-dinitrobenzamide (***20***) white amorphous solid; 54.22% yield; TLC (7 : 3 hexane/EtOAc); $R_f = 0.66$; m.p.: 205.1–205.8°C (lit. 212–213°C [43]); IR υmax (KBr, cm^{-1}): 3297, 3109, 2941, 1646, 1542 and 1345; ^{1}H NMR (500 MHz, DMSO-d6): δ_H 9.05 (*d*; $J = 2.1$ Hz; 2H), 8.94 (*t*; $J = 2.1$ Hz; 1H), 3.81 (*quint*; $J = 3.6$ Hz; 1H), 1.87–1.61 (*m*; 6H), 1.39–1.31 (*m*; 4H); ^{13}C NMR (125 MHz, DMSO-d6): δ_C 161.18, 148.17, 137.31, 127.59, 120.71, 49.18, 32.25, 25.25, 24.91 [44].

N-(4-Methoxybenzyl)-3,5-dinitrobenzamide (***21***) yellow crystal solid; 63.58% yield; TLC (7 : 3 hexane/EtOAc); $R_f = 0.46$; m.p.: 142.4–143.1°C (lit. 155–157°C, [42]); IR υmax (KBr, cm^{-1}): 3303, 3095, 2934, 1643, 1541 and 1344; ^{1}H NMR (400 MHz, DMSO-d6): δ_H 9,66 (*t*; $J = 5.7$ Hz; 1H) 9.08 (*d*; $J = 2.1$ Hz; 2H), 8.95 (*t*; $J = 2.1$ Hz; 1H), 7.29 (*d*; $J = 8.7$ Hz; 2H), 6.90 (*d*; $J = 8.7$ Hz; 2H), 4.47 (*d*; $J = 5.8$ Hz; 2H), 3.73 (s; 3H); ^{13}C NMR (101 MHz, DMSO-d6): δ_C 162.03, 158.46, 148.24, 136.91, 130.67, 129.02, 127.59, 120.87, 113.82, 55.12, 42.71 [42].

2.2. Microbiological Assay. The reference strains of *Candida* spp. used in this study were obtained from the Central Bureau voor Schimmelcultures (CBS): *Candida albicans* CBS 562, *Candida krusei* CBS 573, and *Candida tropicalis* CBS 94. Nystatin, tween 80%, DMSO, caspofungin diacetate, and ergosterol were obtained from Sigma-Aldrich® Chemical Co. (St. Louis, MO, USA), and sorbitol (D-sorbitol anhydrous) from INLAB® (São Paulo, Brazil). All assays were performed in triplicate in three independent experiments.

2.2.1. Minimum Inhibitory Concentration (MIC). Minimum Inhibitory Concentration tests were performed using microdilution technique in 96-well plates, as specified by the Clinical and Laboratory Standards Institute (CLSI) [45]. Through serial dilutions, concentrations of the evaluated products were obtained, ranging from 1000 μg/mL to 7.8 μg/mL. The products were solubilized in 5% DMSO in distilled and sterilized water. 100 μL of the fungal strain inoculum was then added to all wells, resulting in a final cell concentration of 2.5×10^3 CFU/mL. Controls were performed for culture medium sterility and fungal growth

viability. The 5% DMSO solution was tested to evaluate potential interference in microbial growth inhibition. Nystatin was used as a positive control [46]. The plates were incubated at 35 ± 2°C for 24 hours, and to confirm cell viability after the incubation period, 2,3,5-triphenyltetrazolium chloride (1%) (Sigma-Aldrich®) (TTC) was added [47]. The MIC was defined as the lowest concentration capable of inhibiting fungal growth (absence of turbidity of the culture medium) [45]. Considering that the pharmacological potency of the synthesized molecules can be amplified using chemical modifications in their structures, the bioactivity of the compounds was determined from the MIC values and then classified according to the following categories: a) very strong bioactivity (MIC <10 μg/mL); b) strong bioactivity (MIC between 10 and 25 μg/mL); c) good bioactivity (MIC between 26 and 125 μg/mL); d) moderate bioactivity (MIC from 126 to 500 μg/mL); e) mild bioactivity (MIC in the range of 501–1000 μg/mL); and f) absence of bioactivity (MIC >1000 μg/mL) [48].

2.2.2. Minimum Fungistatic Concentration (MFC). MFC was determined using subculture aliquots (30 μL), from the wells corresponding to the MIC (and higher concentrations) on Sabouraud Dextrose agar (KASVI1, Kasv Imp and Dist. Prod/Laboratórios LTDA, Curitiba, Brazil). The plates were incubated for 48 hours at 35°C ± 2°C, and reading was performed by visual observation of fungal growth based on counting of Colony-Forming Units (CFU). The MFC/MIC ratio was calculated to determine whether the substance presented fungistatic (MFC/MIC ≥4) or fungicidal (MFC/MIC <4) activity [49].

2.2.3. Mechanism of Action: Ester Antifungal Activity

(1) Sorbitol Assay. To define the possible mechanism of action of esters 1 and 2 on the *Candida albicans* cell wall, the microdilution test was performed in the presence of Sorbitol (D-sorbitol—anhydrous) INLAB Laboratory. An inoculum was prepared with sorbitol at a final concentration of 0.8 M. The plates were aseptically sealed and incubated at 35 ± 2°C for 48 hours. Caspofungin was used as a positive control at an initial concentration of 1 μg/mL [50–52].

(2) Ergosterol Assay. The ergosterol assay was conducted to evaluate the possible effect of the products on the fungal cell membrane and used the microdilution method, as described above. The inoculum was prepared with ergosterol at a concentration of 400 μg/ml (1008.44 μM). The plates were incubated at a temperature of 35 ± 2°C for 48 hours. Nystatin was used as a positive control at an initial concentration of 120 μg/mL [50–54].

2.3. Molecular Modeling

2.3.1. Targets Selection. The potential molecular targets of compound 2 were selected following two approaches. Based on the experimental results, the first of these consisted in the selection of the proteins involved in ergosterol synthesis. These receptors were defined from the information available at the *Candida* Genome Database (Pathway PWY3B3-3) [55]. The second set of potential targets of compound 2 was selected from a homology-based computational target fishing approach. For the latter, the compound was used as input to the Similarity Ensemble Approach (SEA) web server [56] to predict its possible targets. Given that target fishing approaches are biased against ligand-receptor interactions in humans, the homology of the predicted targets in *C. albicans* was identified through a Blast search [57]. This search took as input the sequences of the SEA predicted targets and was performed against the *C. albicans* (taxid 5476) proteins present in the Reference proteins database (refseq_protein) through the NCBI Blast server implementation (https://blast.ncbi.nlm.nih.gov/). Any *C. albicans* protein identical in at least 35% to any of the query sequences and covered by the Blast alignment in more than 85% of its length was selected as a potential target of compound 2.

2.3.2. Molecular Docking. Molecular docking calculations were performed as previously described in our previous publications [58–60]. Shortly, the lowest energy 3D conformer of the compound was generated, and am1-bcc partial atomic charges were added to it with OpenEye's software Omega [61] and MolCharge [62], respectively. The Merck Molecular Force Field (MMFF94), as implemented in Omega, was used to obtain the compound conformer using default parameters. The crystal structures of the HSP90 (code 6CJR), MEP2 (code 5AF1), and ERG11 (code 5TZ1) molecular targets were retrieved from the Protein Data Bank database [63]. For the rest of the explored receptors that lack experimental 3D structures, homology models were obtained through the SWISS-MODEL server [64]. All water molecules were removed from the receptors for molecular docking, and only functionally relevant cofactor and metal atoms were retained in them.

All docking calculations were performed with the Gold software [65]. The ligand binding sites were defined as any residue within 6 Å from the cocrystalized ligand or the ligands present in the template structures used to build the homology models. In case that no reference ligand was present, a reference point was manually defined withing the binding cavity, and any amino acid at a distance lower than 10 Å from it was selected for the binding cavity. Primary orientation and scoring were performed with the CHEMPLP scoring function, and 30 different binding poses were predicted for each receptor. These predicted orientations of compound 2 in each receptor were rescored with the GoldScore, ChemScore, and ASP scoring functions. The residues side chains pointing toward the binding cavity were regarded as flexible for molecular docking. Furthermore, the search efficiency parameter of gold is set to 200% (very flexible), and the ligand was considered as flexible for docking studies.

The most probable binding modes of the ligand to each receptor were determined from a consensus scoring method that considers the scores values provided by the four scoring functions employed. This consensus score is computed as follows:

$$Z_i = \frac{\sum_j S_{i,j} - \overline{S_j}/st\ d(S_j)}{4}, \quad (1)$$

where $S_{i,j}$ is the score of ligand pose i according to scoring function j, $st\ d(S_j)$ is the standard deviation of the $S_{i,j}$ values, and $\overline{S_j}$ is their average.

2.3.3. Molecular Dynamics Simulations and Estimation of the Free Energies of Binding. Molecular dynamics (MD) simulations and the estimation of the free energies of binding were performed with Amber 18 [66] as described in our previous publication [60]. Briefly, the Amber force fields ff14SB and gaff were used to parametrize proteins and compound 2, respectively. All the complexes, except those containing MEP2 that is a membrane protein, underwent the same preparation protocol that included energy minimization, heating, and equilibration.

The systems containing soluble proteins were enclosed in truncated octahedron boxes and solvated with TIP3P water molecules, and the excess charge was neutralized by the addition of either Na^+ (for systems with negative formal charge) or Cl^- (for systems with positive formal charge) counterions. The prepared systems were energy minimized in two steps at constant volume and with long-range electrostatic interactions treated with the Particle Mesh Ewald (PME) method. The first of these consisted in 500 steps of the steepest descent method followed by 500 cycles of conjugate gradient. During the second energy minimization stage, 500 steps of the steepest descent algorithm followed by 1000 cycles of conjugate gradient were applied. All atoms except the solvent and the counterions were constrained with a force constant of 500 kcal/mol·Å^2 during the first energy minimization step, while no constraint was applied during the second one.

The energy minimized systems were heated from 0 K to 300 K during 20 ps, keeping the solute constrained with a force constant of 10 kcal/mol·Å^2. From this step on, temperature was controlled by a Langevin thermostat with a collision frequency of 1.0 ps^{-1}, and the bonds involving hydrogen atoms were constrained with the SHAKE algorithm. Next, the systems were equilibrated for 100 ps at constant temperature (300 K) and constant pressure (1 bar). Pressure was controlled with isotropic position scaling setting a relaxation time of 2 ps during equilibration. Production runs were set to 2 ns using the same parameters as during the equilibration stage. In total, 20 of these short 2 ns MD simulations were run for each system taking as input the last snapshot of the equilibration process and with different random initial velocities per simulation.

On the other hand, the complexes of compound 2 with MEP2 were prepared with the CHARMM-GUI server [67, 68]. These systems were integrated in a bilayer membrane containing, on each side, 25 cholesterol (CHL), 50 1-Palmitoyl-2-oleoylphosphatidylethanolamine (POPE), and 50 1-Palmitoyl-2-oleoylphosphatidylcholine (POPC) molecules. The systems containing the complex and the membrane were enclosed in a rectangular box and solvated with TIP3P water molecules, and any excess charge was neutralized by the addition of K^+ and Cl^- ions. The configuration files provided by the CHARMM-GUI server were used for the energy minimization, heating, and equilibration of these systems. As for the soluble proteins, the complexes with MEP2 were subject to 20 MD simulations of 2 ns length each one.

The free energies of binding of compound 2 to all targets were estimated with the MM-PBSA method implemented in Amber [69]. These calculations were performed over 200 MD snapshots that were selected one every 200 ps from the 40 ns MD simulations performed for each complex. The ionic strength for MM-PBSA calculations was set to 0.100 mM. For the complexes with MEP2, the implicit membrane model available in Amber was employed, and the membrane dielectric factor set to 4.

3. Results and Discussion

For the present study, a series of twenty 3,5-dinitrobenzoic acid (1) derivatives (Scheme 1) was prepared: ethyl 3,5-dinitrobenzoate (**2**), n-propyl 3,5-dinitrobenzoate (**3**), isopropyl 3,5-dinitrobenzoate (**4**), butyl 3,5-dinitrobenzoate (**5**), pentyl 3,5-dinitrobenzoate (**6**), isopentyl 3,5-dinitrobenzoate (**7**), decyl 3,5-dinitrobenzoate (**8**), 4-Chlorobenzyl 3,5-dinitrobenzoate (**9**), benzyl 3,5-dinitrobenzoate (**10**), 4-methoxy-benzyl 3,5-dinitrobenzoate (**11**), 4-isopropyl-benzyl 3,5-dinitrobenzoate (**12**), 4-nitro-benzyl 3,5-dinitrobenzoate (**13**), 3-methoxy-benzyl 3,5-dinitrobenzoate (**14**), *N*-benzyl-3,5-dinitrobenzamide (**15**), *N*,*N*-diethyl-3,5-dinitrobenzamide (**16**), 3,5-dinitrobenzamide *N*-phenyl-benzamide (**17**), *N*-(4-chlorobenzyl)-3,5-dinitrobenzamide (**18**), *N*-(4-fluorobenzyl)-3,5-dinitrobenzamide (**19**), *N*-cyclohexyl-3,5-dinitrobenzamide (**20**) and *N*-(4-methoxybenzyl)-3,5-dinitrobenzamide (**21**).

The esters and amides synthesized are structurally related, and the benzoyl structure disubstituted with NO_2 (nitro group) in positions 3 and 5 was maintained, varying only the oxygen attached substituent in the ester function, and nitrogen attached substituent in the amide function. The ^{1}H and ^{13}C NMR spectra of the synthesized products demonstrated the presence of 3 hydrogens (H-2, H-4, and H-6) attached to the aromatic ring; and 7 carbons in common (C-1, C-2, C-3, C-4, C-5, C-6, and C=O), being 6 (six) on the aromatic ring, and 1 (one) referring to either the ester or amide carbonyl.

All of the synthesized esters and amides were evaluated for *in vitro* antifungal activity against strains of *Candida albicans*, *Candida krusei*, and *Candida tropicalis* (Table 1). Of the twenty derivatives tested, fungicidal activity against at least one of the tested strains was observed for ten (50%), with emphasis on four compounds (**2**, **3**, **9**, and **16**), which presented activity against all of the tested strains and greater antifungal potency than the starting compound 3,5-dinitrobenzoic acid (**1**).

The effect of the alkyl-substituted ester group (*R*) on activity against *Candida* strains is evident. In the series studied, short linear alkyl chains potentiated biological activity, while larger alkyl groups resulted in a lower activity. Thus, ethyl 3,5-dinitrobenzoate ester (compound **2**: ethyl

Table 1: Minimal inhibitory and fungicidal concentrations (MFC/MIC) of 3,5-dinitrobenzoic acid and its derivatives expressed in μg/mL and mM.

Compounds	*Candida albicans* (CBS 562)			*Candida krusei* (CBS 573)			*Candida tropicalis* (CBS 94)		
	MIC (μg/mL)/(mM)	MFC (μg/mL)/(mM)	MFC/MIC	MIC(μg/mL)/(mM)	MFC(μg/mL)/(mM)	MFC/MIC	MIC(μg/mL)/(mM)	MFC(μg/mL)/(mM)	MFC/MIC
1	1000/4.71	1000/4.71	1	1000/4.71	1000/4.71	1	1000/4.71	1000/4.71	1
2	125/0.52	250/1.04	2	1000/4.16	1000/4.16	1	500/2.08	500/2.08	1
3	250/0.98	500/1.96	2	1000/3.92	1000/3.92	1	500/1.96	500/1.96	1
4	>1000/3.92	>1000/3.92		1000/3.92	1000/3.92	1	>1000/3.92	>1000/3.92	
5	1000/3.73	1000/3.73	1	1000/3.73	1000/3.73	1	>1000/3.73	>1000/3.73	
6	1000/3.54	1000/3.54	1	>1000/3.54	>1000/3.54		>1000/3.54	>1000/3.54	
7	>1000/3.54	>1000/3.54		>1000/3.54	>1000/3.54		>1000/3.54	>1000/3.54	
8	1000/2.83	1000/2.83	1	>1000/2.83	>1000/2.83		>1000/2.83	>1000/2.83	
9	1000/2.97	1000/2.97	1	250/0.74	250/0.74	1	1000/2.97	1000/2.97	1
10	>1000/3.30	>1000/3.30		>1000/3.30	>1000/3.30		>1000/3.30	>1000/3.30	
11	>1000/3.01	>1000/3.01		1000/3.01	1000/3.01	1	>1000/3.01	>1000/3.01	
12	>1000/2.90	>1000/2.90		1000/2.90	1000/2.90	1	>1000/2.90	>1000/2.90	
13	>1000/2.88	>1000/2.88		>1000/2.88	>1000/2.88		>1000/2.88	>1000/2.88	
14	>1000/3.01	>1000/3.01		>1000/3.01	>1000/3.01		>1000/3.01	>1000/3.01	
15	>1000/3.32	>1000/3.32		>1000/3.32	>1000/3.32		>1000/3.32	>1000/3.32	
16	1000/3.74	1000/3.74	1	1000/3.74	1000/3.74	1	1000/3.74	1000/3.74	1
17	>1000/3.48	>1000/3.48		>1000/3.48	>1000/3.48		>1000/3.48	>1000/3.48	
18	>1000/2.98	>1000/2.98		>1000/2.98	>1000/2.98		>1000/2.98	>1000/2.98	
19	>1000/3.13	>1000/3.13		>1000/3.13	>1000/3.13		>1000/3.13	>1000/3.13	
20	>1000/3.41	>1000/3.41		>1000/3.41	>1000/3.41		>1000/3.41	>1000/3.41	
21	>1000/3.02	>1000/3.02		>1000/3.02	>1000/3.02		>1000/3.02	>1000/3.02	
Nystatin	3.75/0.0040	3.75/0.0040	1	3.75/0.0040	3.75/0.0040	1	3.75/0.0040	3.75/0.0040	1
Control medium	−			−			−		
Fungal growth control	+			+			+		
5% DMSO solution	+			+			+		

(+) indicates growth of the microorganism. (−): no growth of the microorganism.

group) was the most bioactive compound for the *Candida albicans* (MIC = 0.52 mM), *Candida krusei* (MIC = 4.16 mM), and *Candida tropicalis* (MIC = 2.08 mM) strains, followed by compound **3**: propyl group, which also showed excellent activity against *Candida* strains. The presence of an isopropyl group in ester **4** contributed to its bioactivity against *Candida krusei* (MIC = 3.92 mM).

The comparison of compound **2** with compound **5** (*n*-butane group) suggests that the increase in the carbon chain in the ester compound **5** resulted in inactivity against *Candida tropicalis* and reduced potency against other strains. Within the series studied, medium-sized linear alkyl chains demonstrated antifungal activity, while branched alkyl groups showed no activity. Thus, compound **6** presented activity against *Candida albicans* (MIC = 3.54 mM), while its analogue, compound **7** (isopentyl group), presented no antifungal activity. Compound **8**, with a long linear alkyl chain (10 carbon atoms), only presented activity against *Candida albicans* (MIC = 2.83 mM).

Compounds presenting aryl radicals demonstrated either reductions or an absence of antifungal activity. Specifically, insertion of a benzyl group (compounds **10** and **15**) led to a total loss of antifungal activity. However, in the ester **9**, the presence of an electron-withdrawing group, such as chlorine, contributed to antifungal activity against all strains tested. Lima et al., [70] observed that the presence of a chlorosubstituent resulted in an increase in the antifungal activity in esters derived from cinnamic and benzoic acids. Interestingly, the presence of chlorine in the *para* position of its analogue, amide **18**, did not favor antifungal activity.

The comparison of amide **18** with amide **19** revealed that switching the chlorosubstituent (**18**) with fluorine (**19**) in the *para* position of the aromatic ring did not yield bioactivity. However, Oliveira et al. [71] used vanillic acid as a starting material to prepare an amide containing a fluorine substituent in the *para* position, and the substituent favored activity against the tested *Candida* strains.

4-Methoxy-benzyl 3,5-dinitrobenzoate **(11)** presents an aromatic ring with an electron-donating group, methoxy in the *para* position displayed activity against *Candida krusei* (MIC = 3.01 mM), while the derivative **14** (with an MeO group in the *meta* position) presented no antifungal activity. This demonstrates the importance for antifungal activity of a substituent in the *para* position. In contrast, when comparing compound **11** with its analogue, the amide **21**, the inserted substituent (MeO group in the *para* position) did not promote antifungal activity.

Ester **12**, which possesses an aromatic ring with an isopropyl substituent, also presented activity against *Candida krusei* (MIC = 2.90 mM). However, the introduction of a nitro group at the *para* position resulted in a loss of activity for 4-nitro-benzyl 3,5-dinitrobenzoate (**13**). When

Table 2: MIC values in (μg/mL) and (mM) of esters **2** and **3** in the absence and presence of sorbitol (0.8 M) and ergosterol against *Candida albicans*.

Compound	Concentration (μg/mL)/(mM)	*Candida albicans* (CBS 562)		*Candida albicans* (CBS 562)	
		Without sorbitol (μg/mL)/(mM)	With sorbitol (μg/mL)/(mM)	Without ergosterol (μg/mL)/(mM)	With ergosterol (μg/mL)/(mM)
2	1000/4.16	−	−	−	−
	500/2.08	−	−	−	−
	250/1.04	−	−	−	−
	125/0.52	−	−	−	+
	62.5/0.26	+	+	+	+
	31.25/0.13	+	+	+	+
3	1000/3.92	−	−	−	−
	500/1.96	−	−	−	+
	250/0.98	−	−	−	+
	125/0.49	+	+	+	+
	62.5/0.24	+	+	+	+
	31.25/0.12	+	+	+	+
Nystatin	120/0.128			−	−
	60/0.064			−	−
	30/0.032			−	+
	15/0.016			−	+
	7.5/0.008			−	+
	3.75/0.0040			−	+
	1.87/0.002			+	+
	0.93/0.001			+	+
Caspofungin	1/0.000896	−	−		
	0.5/0.000448	−	−		
	0.25/0.000224	−	+		
	0.125/0.000112	−	+		
	0.0625/0.000056	−	+		
	0.031/0.000028	−	+		
	0.015/0.000014	+	+		

(+) indicates growth of the microorganism. (−): no growth of the microorganism.

comparing esters **9**, **10**, **11**, **12**, **13**, and **14**, we verified that changes in aromatic ring substitutions promote changes in antifungal activity.

Amide **16** presented activity against *Candida albicans* (MIC = 3.74 mM), *Candida krusei* (MIC = 3.74 mM), and *Candida tropicalis* (MIC = 3.74 mM). The data indicate that the presence of less bulky groups in the *R* side chain of this amide contributes to its bioactivity.

Despite the literature reporting biological activity for various amides against *Candida* species [71, 72], most of the amides evaluated (**15**, **17**, **18**, **19**, **20**, and **21**) presented no antifungal activity. This data suggests that the 3,5-dinitrobenzoyl substructure is not promising for amide derivatives.

The results also revealed that the compounds were more active against strains of *Candida albicans*. However, products **4**, **11**, and **12** were bioactive only against *Candida krusei*. The MFC/MIC ratio of the compounds revealed that all present fungicidal biological activity [69]. In general, against strains of the *Candida* genus, the esters presented a better antifungal activity profile than the amides.

The compounds presenting the greatest biological activity (compounds **2** and **3**) were submitted to tests to elucidate possible mechanisms of action against *Candida albicans* strains, using ergosterol and sorbitol to determine their likely pharmacological targets (Table 2).

Ergosterol is a component of the fungal cell membrane that is important for membrane fluidity and integrity. It is a target for drugs that directly bind to ergosterol or inhibit its biosynthesis, such as polyenes and azoles, respectively [50]. Our results demonstrated that when ergosterol was added to the medium containing the microorganism and compound 3, a significant increase in MIC (3.92 mM) occurred, indicating that the compound possibly acts by altering the physiological functions that involve the presence of ergosterol in the cell membrane. Compound **2** also presented an increase in MIC (1.04 mM) in the presence of ergosterol, indicating that its mechanism of action may also involve ergosterol in the fungal membrane.

Sorbitol is recognized as an osmotic protector of fungal cell walls, and when added to the culture medium in *in vitro* tests, it protects the cell from damage caused by drugs that act by inhibiting cell wall synthesis, being formed by chitin and glycan [73]. In this study, in the presence of sorbitol, no change was observed in the MIC values of either compound **2** or **3**, indicating that their probable mechanism of action is not related to changes in cell wall function.

To the best of our knowledge, there is no previous information about the molecular targets of 3,5-dinitrobenzoate derivatives in *C. albicans*. A literature survey for the antifungal mechanism of action of this type of compound returned no results. In addition, the experimental

Table 3: Potential targets of compound **2** in *C. albicans* selected for modeling studies.

C. albicans target[a]	Description	ID
Q59NQ5_CANAL[b]	Glutathione reductase	GLR1
HSP60_CANAL[b]	Heat shock protein 60	HSP60
Q59UP8_CANAL[b]	Ammonium transporter	MEP2
DCOR_CANAL[b]	Ornithine decarboxylase	SPE1
ERG1_CANAL[b],[c]	Squalene monooxygenase	ERG1
KMO_CANAL[b]	Kynurenine 3-monooxygenase	BNA4
A0A1D8PJI5_CANAL[b]	Arylsulfatase	atsA
HSP90_CANAL[b]	Heat shock protein 90	HSP90
A0A1D8PCB9_CANAL[c]	C-8 sterol isomerase	ERG2
ERG6_CANAL[c]	Sterol 24-C-methyltransferase	ERG6
ERG7_CANAL[c]	Lanosterol synthase	ERG7
A0A1D8PI71_CANAL[c]	Bifunctional farnesyl-diphosphate farnesyltransferase/squalene synthase	ERG9
A0A1D8PH52_CANAL[c]	Acetyl-CoA C-acetyltransferase	ERG10
CP51_CANAL[c]	Lanosterol 14-alpha demethylase	ERG11
A0A1D8PEL1_CANAL[c]	Mevalonate kinase	ERG12
A0A1D8PTW6_CANAL[c]	3-Hydroxy-3-methylglutaryl coenzyme a synthase	ERG13
A0A1D8PH78_CANAL[c]	Bifunctional (2E,6 E)-farnesyl diphosphate synthase/dimethylallyltranstransferase	ERG20
A0A1D8PD39_CANAL[c]	3-Hydroxy-3-methylglutaryl coenzyme a reductase	HMG1
A0A1D8PLI2_CANAL[c]	Isopentenyl-diphosphate delta-isomerase	IDI1
A0A1D8PC43_CANAL[c]	Diphosphomevalonate decarboxylase	MVD

(a) UniProt entry name. (b) Predicted from the computational target fishing approach. (c) Part of the ergosterol synthesis pathway.

results reported here confirm that compound **2** interferes with the synthesis of ergosterol in *C. albicans*. For this reason, computational modeling was performed with the objective of identifying probable targets of compound **2** that could explain its antifungal activity. Instead of focusing only on the proteins involved in the synthesis of ergosterol in the fungus, we also included other potential molecular targets that were selected following the homology-based target fishing approach described in the Methods section.

The potential targets of compound **2** in *C. albicans* are provided as Supplementary Materials in Table S1. From the 32 initially selected proteins, 12 were excluded from the modeling process due to diverse reasons. These were related to the poor quality of the predicted homology models, the lack of information about the mechanisms of the proteins, and hence regarding their potential inhibition, and the obtaining of homology models for only a small fragment of the target sequence. The list of the 20 receptors selected for modeling studies is given in Table 3. Among these, eight covering different biological processes were identified by the computational target fishing approach. On the other hand, the remaining 12 proteins belong to the ergosterol biosynthesis pathway in *C. albicans*. Also, ERG1 that belongs to the ergosterol synthetic pathway was also retrieved from target fishing predictions.

The protocol described in the Methods section was applied to dock compound **2** into the binding sites of the proteins listed in Table 3. The full results of the molecular docking studies are provided as Supplementary Materials in Table S2. The visual inspection of the predicted complexes listed in Table S2 reveals meaningful interactions between the ligand and the receptors, with the ligand inside the respective binding cavities. If the same consensus scoring scheme used for the selection of the most probable ligand poses is applied to those listed in Table S2, it can be concluded that the top scored targets are HSP90, ERG11, ERG20, ERG9, and ERG1. On the other hand, the list of receptors with the worst predictions include GLR1, HMG1, atsA, MEP2, and MVD. Overall, 40 different ligand-receptor complexes were identified through molecular docking calculations with an average of 2 possible orientations of compound **2** in the binding site of each studied receptor.

It has been shown that the refinement of molecular docking models with MD simulations and the estimation of their free energies of binding is a valuable approach to further refine the list of potential targets of bioactive compounds [58–60]. Taking this into account, the free energies of binding of compound **2** to the proteins listed in Table 3 were computed as described in the Methods section. The detailed results of the MM-PBSA calculations are provided as Supplementary Materials in Table S3 and these are summarized in Figure 1. The figure represents the ligand pose with the lowest predicted value of ΔG of binding for each molecular target used for modeling.

The predictions of the free energies of binding show that the complexes formed by compound **2** with most of the evaluated targets are feasible ($\Delta G < 0$). Only the GLR1, SPE1, MVD, ERG2, HSP60, and IDI1 proteins are predicted to form unstable complexes with the ligand. On the other hand, the lowest values of the ΔG of binding are obtained for the MEP2, HSP90, BNA4, ERG20, and ERG1 targets. It is interesting to note that the three top ranked targets (MEP2, HSP90, and BNA4) were predicted through the target fishing approach and are not part of the ergosterol biosynthesis pathway in *C. albicans*. Furthermore, among the 13 molecular targets for which the predicted free energies of binding are lower than -3 kcal/mol, 10 are directly linked to the ergosterol synthesis. Overall, the modeling results agree with the experimental observations that compound **2** reduces ergosterol levels in the fungus but also points to

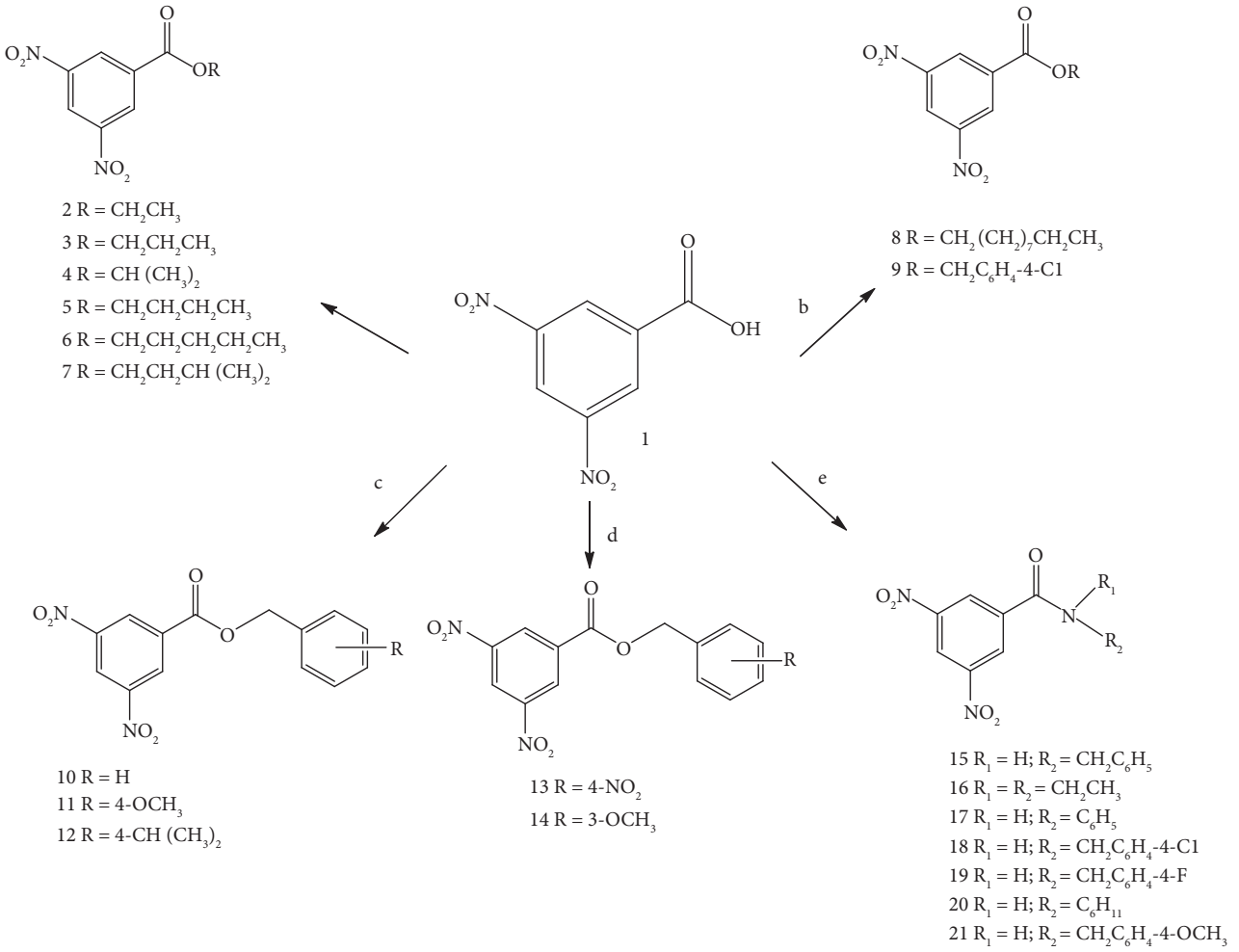

Scheme 1: Synthesis of esters and amides derived from 3,5-dinitrobenzoic acid: (a) ROH, H_2SO_4, reflux; (b) Et_3N, RX, acetone, reflux; (c) ROH, THF, TPP, DIAD, 0°C to r.t. (d) (I) $SOCl_2$, reflux; (II) ROH, CH_2Cl_2, 0°C to r.t. (e) (I) $SOCl_2$, reflux; (II) RNH_2, Et_3N, CH_2Cl_2, 0°C to r.t.

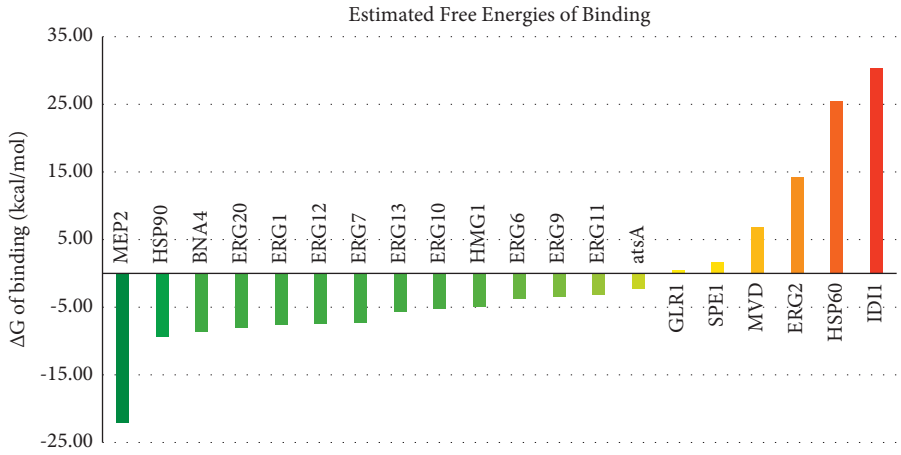

Figure 1: Predicted free energies of binding of compound **2** to its potential targets ranked from best ΔG of binding (green) to worst (red).

possible alternative mechanism of actions. Based on the modeling results, we decided to further investigate the predicted complexes of the compound with the MEP2, HSP90, ERG20, ERG1, ERG12, and ERG7 targets. The first two are not directly related to the ergosterol synthesis pathway, while the rest of them are part of it.

The predicted binding modes of compound **2** to the MEP2 and HSP90 targets are shown in Figure 2. The

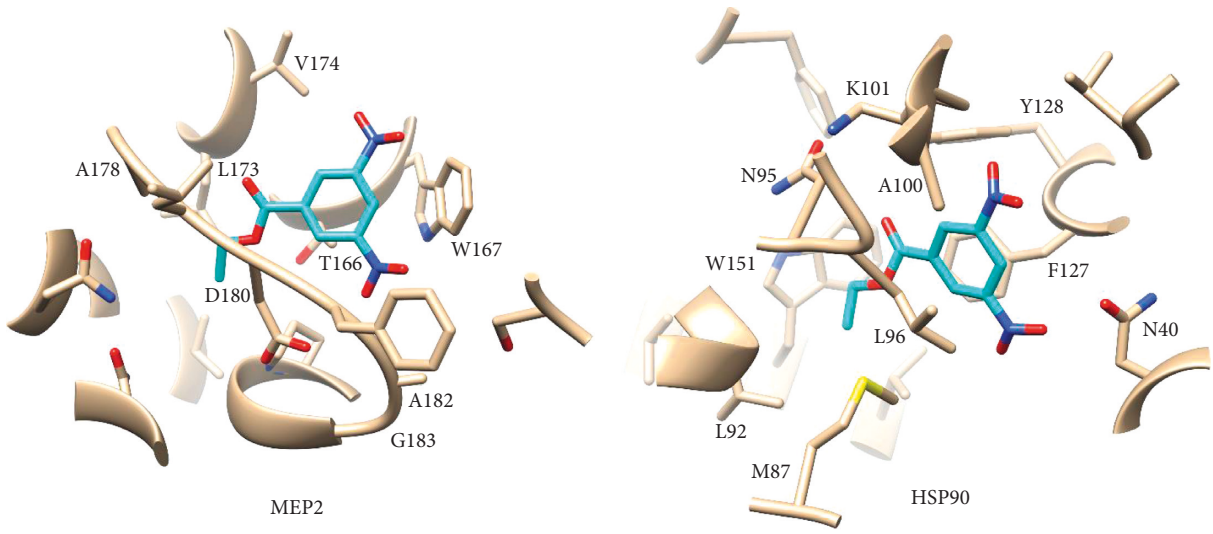

Figure 2: The predicted binding modes of compound **2** to the MEP2 (left) and HSP90 (right) targets. Receptors are depicted in gray and the ligand in cyan. The non-carbon atoms are colored as red for oxygen, blue for nitrogen, and yellow for sulfur. Only residues interacting with compound **2** in more than 50% of the analyzed MD snapshots are labelled in the figure.

structures represented in the figures were selected as the centroids of the most populated clusters obtained from grouping the conformers of the ligand along the 200 MD snapshots used for MM-PBSA calculations. All images containing molecular structures were produced with UCSF Chimera [74]. The predicted ligand-receptor networks of interactions are provided as Supplementary Materials in Figure S7 and were obtained with Cytoscape [75].

Compound **2** is predicted to interact with both MEP2 and HSP90 mainly through Van der Waals and hydrophobic interactions. For MEP2, no hydrogen bond is predicted to form in the complex, while for HSP90, the ligand hydrogen bonds to Y128 in a small fraction (17%) of the analyzed MD snapshots. A common feature to both complexes is that the phenyl ring of the ligand stacks in front of aromatic amino acids, W167 of MEP2 and F127 of HSP90. We hypothesize that these π–π stacking interactions serve as anchor for binding and have a determinant contribution to the stabilization of the complexes.

In MEP2, compound **2** is predicted to orientate with one of its nitro groups pointing to the entrance of the cavity, while the other one, as well as the ester moiety, orientates toward the bottom of the ammonium binding channel. In addition to the stacking with W167, the compound also interacts in more than 50% of the analyzed MD snapshots with T166, L173, V174, A178, D180, A182, and G183. In the predicted model of binding to HSP90, compound **2** is orientated with the two nitro groups occupying the entrance of the binding cavity and the ester substituent facing W151 at the bottom of the receptor pocket. The rest of the most frequent interactions of the chemical with HSP90 include N40, M87, L92, N95, L96, A100, K101, and Y128.

The complexes predicted for compound **2** with the ERG20, ERG1 ERG12, and ERG7 targets, which are part of the ergosterol synthesis pathway in *C. albicans*, are shown in Figure 3. Something common to these complexes, as previously observed for MEP2 and HSP90 too, is the stacking of the ligand's phenyl ring in front of aromatic residues of the receptors: F202 of ERG20; F402 and Y77 of ERG1; F54 of ERG12; and F695 and H226 of ERG7. Although more frequent than with the previously discussed targets, little presence of hydrogen bonds with the receptors belonging to the ergosterol pathway is observed. The higher frequency of hydrogen bond interactions among these targets is obtained for ERG1 through the side chains of Q50 and Y77 in 41% of 59% of the analyzed MD snapshots, respectively. Likewise, this type of interaction is observed in 10% and 25% of the analyzed snapshots with the backbone of A114 in ERG12 and with the side chain of K4 in ERG20, respectively. Finally, compound **2** accepts hydrogen bonds from the side chains of Y504 and W224 of ERG7 with low frequency (less than 15%).

Overall, the complexes with ERG20, ERG1, ERG12, and ERG7 are mainly stabilized through Van der Waals and hydrophobic interactions, aside the anchor that we postulate from the π–π stacking interactions between the ligand's phenyl ring and the receptors' aromatic residues. One interesting observation is that compound **2** does not directly interact with the FAD cofactor of ERG1 and instead occupies a hydrophobic subpocket on the other side of the binding cavity. Still, this localization of the ligand interferes with the binding of the substrate to the enzyme. In addition to the previously listed residues, those in contact with compound **2** in the targets involved in ergosterol synthesis are as follows: N53, R54, S57, S201, V206, F235, F342, K345, V346 in ERG20; Q50, I79, V240, L242, L249, L340, T341, F420, L434 in ERG1; D56, I57, Y112, A114, V137, R138, S139, I143, S149, T153, F201 in ERG12; and Y91, M97, W186, W224, T227, G377, F522, I525, N696 in ERG7.

In summary, the modeling results point to a multitarget antifungal mechanism of action for compound **2** in *C. albicans* related to different cellular processes. They are also in agreement with the experimental interference of this compound with the synthesis of ergosterol. Ergosterol

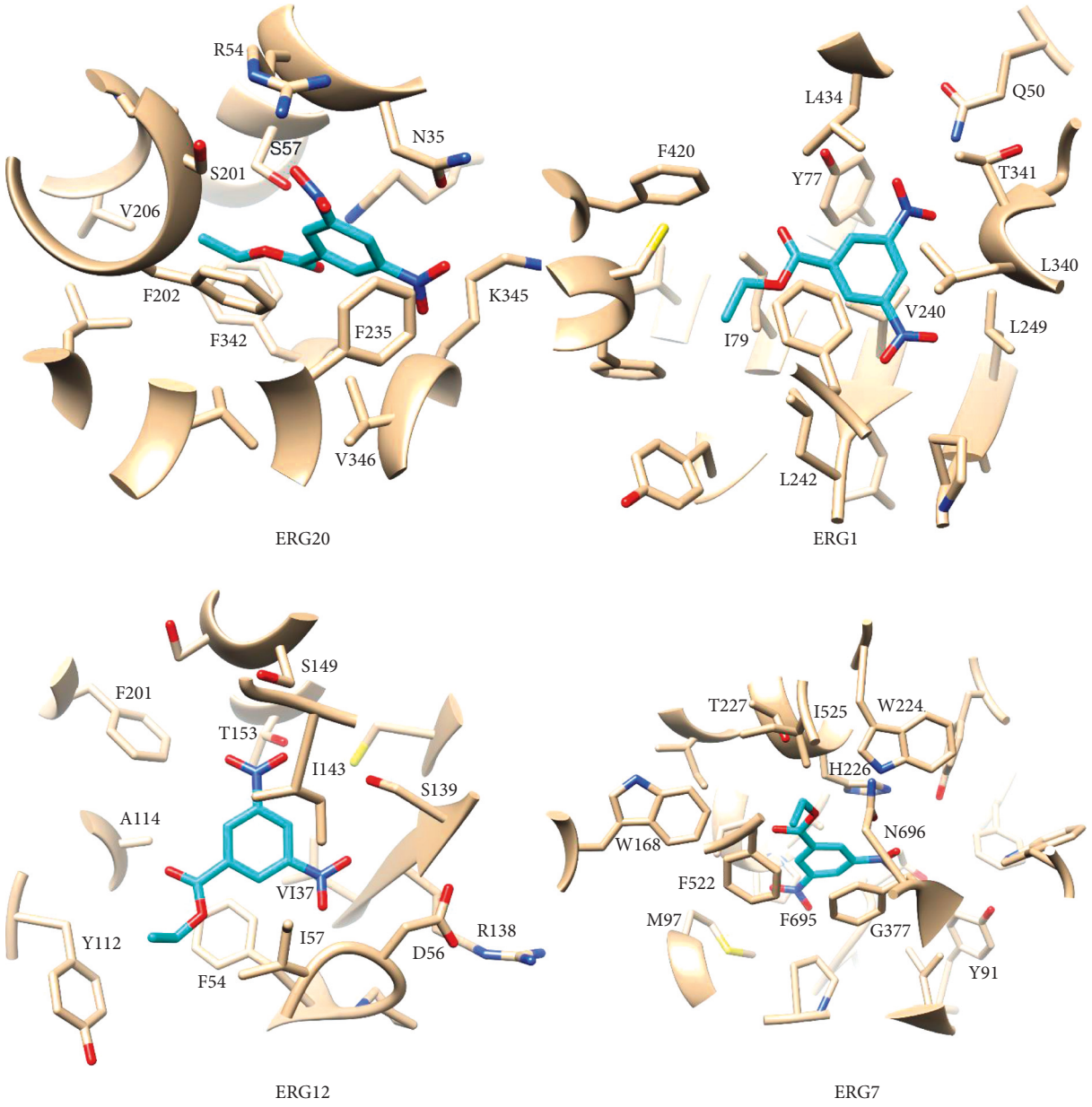

Figure 3: Predicted binding modes of compound **2** to the ERG20 (top left), ERG1 (top right), ERG12 (bottom left), and ERG7 (bottom right) targets. Non-carbon atoms are colored following the scheme: red for oxygen, blue for nitrogen, and yellow for sulfur. Only residues interacting with the compound in more than 50% of the analyzed MD snapshots are labelled in the figure.

synthesis has been shown to be a critical process in *C. albicans*, with ERG20, ERG1, ERG12, and ERG7 previously identified as essential for its growth and virulence and proposed as targets for the development of antifungal drugs [76–80]. Furthermore, MEP2 is an important regulatory component in the development of the fungi, thus making it a potential drug target [81]. Finally, HSP90 has also been validated as a molecular target for antifungal compounds against *C. albicans* [82, 83]. Interestingly, the impairment HSP90 in this fungus results in reduced ergosterol levels through a mechanism that remains to be determined [84].

To further investigate the influence of the substituents on the antifungal activity of the series of compounds, we examined the steric environment of the region where the ethyl group of compound **2** is predicted to bind in each receptor. This is illustrated in Figure 4, where the molecular surfaces of the proteins' regions interacting with the ethyl group of compound **2** are presented. This analysis reveals that this region is sterically constrained in HSP90, ERG7, and ERG20. Thus, large and bulky substituents are not allowed in these subcavities formed in HSP90, ERG7, and ERG20. On the other hand, the regions accommodating the ethyl group can accept larger substituents in ERG1, ERG12, and MEP2. In the case of ERG12, the alkyl chain locates at the entrance of the binding cavity, which provides flexibility on the type of substituents capable of retaining ammonium transport inhibition. The steric limitations observed in the binding cavities of HSP90, ERG7, and ERG20 could explain the better

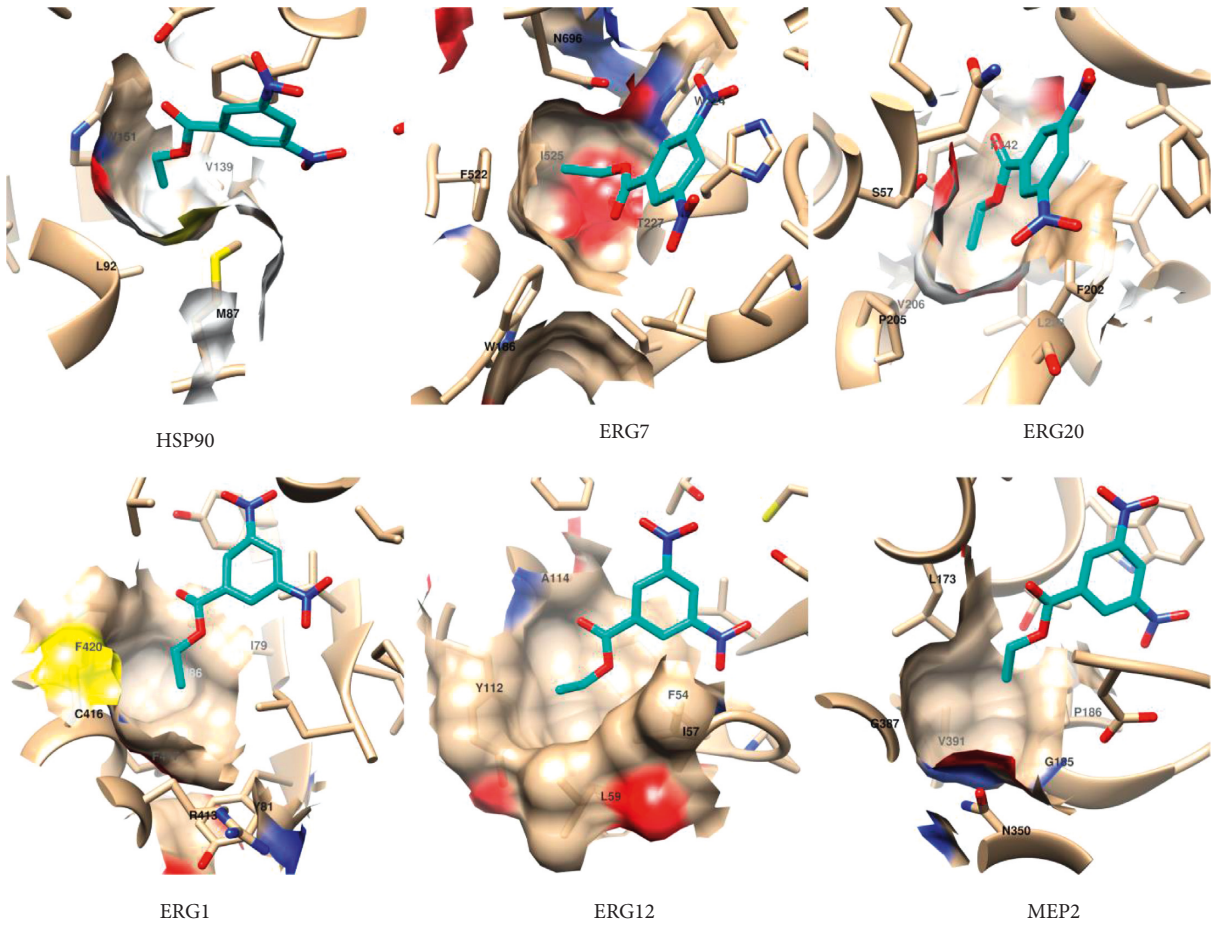

Figure 4: Surface representation of the region of the potential targets of compound **2** interacting with its ethyl group.

Table 4: Physicochemical and ADMET predictions for compound **2** and nystatin.

Parameters	Compound 2	Nystatin
Physicochemical properties		
Molecular weight (g/mol)	240.17	926.09
Rotatable bonds	5	3
H-bond acceptors	6	18
H-bond donors	0	12
Fraction Csp3	0.22	0.7
TPSA (A3)	117.94	319.61
Toxicity		
AMES toxicity	Yes	No
Max. Tolerated dose (human, log(mg/kg/day))	0.003	0.281
hERG I inhibitor	No	No
hERG II inhibitor	No	No
Oral rat acute toxicity (LD50, mol/kg)	2.721	2.518
Oral rat chronic toxicity (LOAEL, log(mg/kg_bw/day))	1.439	2.035
Hepatotoxicity	No	No
Skin sensitization	No	No

antifungal activity of compounds **2** and **3** presenting short linear alkyl chains. That is, short alkyl groups are required to retain the simultaneous binding to the six receptors. In contrast, compounds with bulkier substituents will be unable to bind HSP90, ERG7, and ERG20 but could interact with ERG1, ERG12, and MEP2. In consequence, the observed structure-activity relationships for the series of compounds cannot be explained from only one of its proposed targets. These observations support the proposed multitarget antifungal mechanism of action for compound **2**.

The prediction of the physicochemical properties and toxicity of compound **2** and the reference antifungal nystatin were obtained with the SwissADME and pkCSM web servers, respectively [85,86]. According to the results of these

predictions presented in Table 4, nystatin exceeds the molecular weight and topological polar surface area (TPSA) considered suitable for oral bioavailability. On the other hand, compound **2** is within the advisable region of physicochemical properties and provides room for its optimization without affecting oral bioavailability. The SwissADME server predicts both compounds with 0 PAINS alerts. In terms of toxicity, compound **2** and nystatin are predicted as noninhibitors of hERG I and hERG II as well as nonhepatotoxic and not inducing skin sensitization. One major difference in terms of toxicity is the predicted tolerated doses, with compound **2** having a tolerated dose 100-fold lower than nystatin. Finally, compound **2** is predicted as carcinogenic in contrast to nystatin, possibly linked to the presence of the nitro groups. Overall, the analysis of the physicochemical properties and predicted toxicity of compound **2** indicate that there are opportunities for modifying its physicochemical properties without affecting its oral bioavailability. Furthermore, the experimental evaluation of the mutagenic potential of the compound is required before proceeding to its optimization. Considering that compound **2** is a hit compound, its heat to lead optimization will require considering the improvement of its toxicological profile together with its bioactivity.

Further experimentation is required to fully understand the antifungal mechanism of action of the compounds proposed here. In this sense, our models are valuable tools for guiding and optimizing these forthcoming experiments by providing hypotheses regarding their potential mechanisms of action. In addition, the developed models are useful for the optimization of the potency and selectivity of novel antifungal compounds based on the chemical scaffold herein studied. Along with the improvements in the antifungal activity of 3,5-dinitrobenzoic acid derivatives, their physicochemical and toxicological properties must also be optimized.

4. Conclusions

Using various synthesis methodologies, a collection of 20 esters and amides derived from 3,5-dinitrobenzoic acid was prepared. Antifungal activity tests revealed that derivative **2** presented the best antifungal activity (lower MICs) against *Candida albicans*, *Candida krusei,* and *Candida tropicalis.* This suggests that the insertion of a side chain ethyl group potentiates biological activity. Further, the presence of a propyl group appears to be important for bioactivity since compound **3** also presented strong antifungal activity. Of the series of amides evaluated, only compound **16** presented antifungal activity against the strains tested. Testing for mechanisms of action against *C. albicans* suggests that compounds **2** and **3** interfere with and act by altering physiological functions involving the presence of ergosterol in the cell membrane. The experimental interference observed for compound **2** in ergosterol synthesis suggests a multitarget mechanism of action. The molecular modeling results agreed with this assessment. This study thus presents certain promising prototypes for new antifungal drug development.

Data Availability

The data used to support the findings of this study are available from the corresponding author upon request.

Conflicts of Interest

The authors declare that there are no conflicts of interests regarding the publication of this paper.

Acknowledgments

This work was supported by the Brazilian agencies: National Council for Scientific and Technological Development (CNPq) and Coordination for the Improvement of Higher Education Personnel (CAPES). The authors would like to thank the Multi-User Characterization and Analysis Laboratory (LMCA-UFPB), for the analysis of the nuclear magnetic resonance spectroscopic samples, and the Northeast Strategic Technologies Center (CETENE-UFPE) and the staff Julia Campos, for the high-resolution mass spectroscopic analyses.

Supplementary Materials

Chemical data of synthetic derivatives. Table S1: potential targets of compound **2**. Table S2: results of the molecular docking of compound **2**. Table S3: predicted free energies of binding and their components for the complexes predicted for compound **2**. Figure S7: Predicted network of interactions of compound **2**. (*Supplementary Materials*)

References

[1] H. M. Nakamura, S. M. Caldeira, and M. A. G. Avila, "Incidência de infecções fúngicas em pacientes cirúrgicos: uma abordagem retrospectiva," *Rev. SOBECC*, vol. 18, no. 3, pp. 49–58, 2013.

[2] D. S. Perlin, R. Rautemaa-Richardson, and A. Alastruey-Izquierdo, "The global problem of antifungal resistance: prevalence, mechanisms, and management," *The Lancet Infectious Diseases*, vol. 17, no. 12, pp. e383–e392, 2017.

[3] M. R. Abrantes, E. O. Lima, M. Araújo et al., "Atividade antifúngica de óleos essenciais sobre leveduras *Candida* não," *Albicans. Rev. Bras. Farm*, vol. 94, no. 3, pp. 227–233, 2013.

[4] A. Garcia, Y. Y. Fan, S. Vellanki et al., "Nanoemulsion as an effective treatment against human-pathogenic fungi," *mSphere*, vol. 4, no. 6, p. 19, 2019.

[5] S. Bhattacharya, S. Sae-Tia, and B. C. Fries, "*Candidiasis* and mechanisms of antifungal resistance," *Antibiotics*, vol. 9, no. 6, p. 312, 2020.

[6] S. Campoy and J. L. Adrio, "Antifungals," *Biochemical Pharmacology*, vol. 133, pp. 86–96, 2017.

[7] M. A. Pfaller, "Antifungal drug resistance: mechanisms, epidemiology, and consequences for treatment," *The American Journal of Medicine*, vol. 125, no. 1, pp. S3–S13, 2012.

[8] D. Morii, N. Ichinose, T. Yokozawa, and T. Oda, "Impact of an infectious disease specialist on antifungal use: an interrupted time-series analysis in a tertiary hospital in Tokyo," *Journal of Hospital Infection*, vol. 99, no. 2, pp. 133–138, 2018.

[9] G. Morace, F. Perdoni, and E. Borghi, "Antifungal drug resistance in *Candida* species," *Journal of Global Antimicrobial Resistance*, vol. 2, no. 4, pp. 254–259, 2014.

[10] M. Karabacak, L. Sinha, O. Prasad, Z. Cinar, and M. Cinar, "The spectroscopic (FT-Raman, FT-IR, UV and NMR), molecular electrostatic potential, polarizability and hyperpolarizability, NBO and HOMO-LUMO analysis of monomeric and dimeric structures of 4-chloro-3, 5-dinitrobenzoic acid," *Spectrochimica Acta Part A: Molecular and Biomolecular Spectroscopy*, vol. 93, pp. 33–46, 2012.

[11] C. Dhivya, S. A. A. Vandarkuzhali, and N. Radha, "Antimicrobial activities of nanostructured polyanilines doped with aromatic nitro compounds," *Arabian Journal of Chemistry*, vol. 12, no. 8, pp. 3785–3798, 2019.

[12] R. Parry, S. Nishino, and J. Spain, "Naturally-occurring nitro compounds," *Natural Product Reports*, vol. 28, no. 1, pp. 152–167, 2011.

[13] A. Fries, T. Bretschneider, R. Winkler, and C. Hertweck, "A ribonucleotide reductase-like electron transfer system in the nitroaryl-forming N-oxygenase AurF," *ChemBioChem*, vol. 12, no. 12, pp. 1832–1835, 2011.

[14] F. R. Paulai, S. H. P. Serrano, and L. C. Tavares, "Aspectos mecanísticos da bioatividade e toxicidade de nitrocompostos," *Quimica Nova*, vol. 32, no. 4, pp. 1013–1020, 2009.

[15] L. G. Nascimento, *Preparação de ésteres nitrocinâmicos e avaliação da sua atividade antimicrobiana*, Dissertação, Universidade Federal da Paraíba, João Pessoa, Brazil, 2017.

[16] A. R. Ferreira, *Ésteres sintéticos derivados do ácido 3-metil-4-nitrobenzoico e avaliação da sua atividade antifúngica*, Dissertação, Universidade Federal da Paraíba, João Pessoa, Brazil, 2018.

[17] J. T. Sanderson, H. Clabault, C. Patton et al., "Antiproliferative, antiandrogenic and cytotoxic effects of novel caffeic acid derivatives in LNCaP human androgen-dependent prostate cancer cells," *Bioorganic & Medicinal Chemistry*, vol. 21, no. 22, pp. 7182–7193, 2013.

[18] P. Boeck, M. M. Sá, B. S. d Souza et al., "A simple synthesis of kaurenoic esters and other derivatives and evaluation of their antifungal activity," *Journal of the Brazilian Chemical Society*, vol. 16, no. 6B, pp. 1360–1366, 2005.

[19] W. Li, N. Li, Y. Tang et al., "Biological activity evaluation and structure-activity relationships analysis of ferulic acid and caffeic acid derivatives for anticancer," *Bioorganic & Medicinal Chemistry Letters*, vol. 22, no. 19, pp. 6085–6088, 2012.

[20] J. G Handique, D. Mahanta, A. Devi, and M. P Boruah, "Synthesis and electrochemical behavior of some dendritic polyphenols as antioxidants," *Letters in Organic Chemistry*, vol. 10, no. 1, pp. 53–59, 2013.

[21] X. Y. Ji, H. Q. Wang, L. H. Hao et al., "Synthesis and antiviral activity of N-phenylbenzamide derivatives, a novel class of enterovirus 71 inhibitors," *Molecules*, vol. 18, no. 3, pp. 3630–3640, 2013.

[22] T. Yoshino, S. Imori, and H. Togo, "Efficient esterification of carboxylic acids and phosphonic acids with trialkyl orthoacetate in ionic liquid," *Tetrahedron*, vol. 62, no. 6, pp. 1309–1317, 2006.

[23] G. R. Burns, "The reaction of labeled methanol with carbon monoxide and Hydrogen1," *Journal of the American Chemical Society*, vol. 77, no. 24, pp. 6615-6616, 1955.

[24] L. Fabian, M. Gómez, J. A. Caturelli Kuran, G. Moltrasio, and A. Moglioni, "Efficient microwave-assisted esterification reaction employing methanesulfonic acid supported on alumina as catalyst," *Synthetic Communications*, vol. 44, no. 16, pp. 2386–2392, 2014.

[25] T. Garcia, A. Arrieta, and C. Palomo, "Reagents and synthetic methods 15. Phenyl dichlorophos-phate-dimethylfurmamide complex. A modified one-pot procedure for esterification of carboxylic acids," *Synthetic Communications*, vol. 12, no. 9, pp. 681–690, 1982.

[26] J. R. Sasthav and F. W. Harris, "Internal plasticization of polyimides with alkyl 3, 5-diaminobenzoate compounds," *Polymer*, vol. 36, no. 26, pp. 4911–4917, 1995.

[27] G. B. Malone and E. E. Reid, "The regularities in the melting points of some crystalline derivatives of various aliphatic ALCOHOLS[1]," *Journal of the American Chemical Society*, vol. 51, no. 11, pp. 3424–3427, 1929.

[28] J. Liu, C. Shao, Y. Zhang, G. Shi, and S. Pan, "Copper-catalyzed highly efficient ester formation from carboxylic acids/esters and formates," *Organic and Biomolecular Chemistry*, vol. 12, no. 17, pp. 2637–2640, 2014.

[29] H. Oelschlager and H. Fritsch, "Identification of mono-valent alcohols with 3, 5-dinitrobenzoic anhydride," *Archiv der Pharmazie*, vol. 318, no. 8, pp. 759–763, 1985.

[30] S. Chakraborty, A. Saha, K. Basu, and C. Saha, "Solid-phase benzoylation of phenols and alcohols in microwave reactor: an ecofriendly protocol," *Synthetic Communications*, vol. 45, no. 20, pp. 2331–2343, 2015.

[31] Y. Tsuda, M. Kojima, and J. M. Oh, "Soluble polyimides based on diaminobenzoic acid alkylester," *Polymer Journal*, vol. 38, no. 10, pp. 1043–1054, 2006.

[32] F. Mou, Y. Sun, W. Jin et al., "Reusable ionic liquid-catalyzed oxidative esterification of carboxylic acids with benzylic hydrocarbons via benzylic Csp 3–H bond activation under metal-free conditions," *RSC Advances*, vol. 7, no. 37, pp. 23041–23045, 2017.

[33] P. Toy, T. But, and J. Lu, "Organocatalytic Mitsunobu reactions with 3, 5-dinitrobenzoic acid," *Synlett*, vol. 2010, no. 07, pp. 1115–1117, 2010.

[34] T. L. Amyes and J. P. Richard, "Concurrent stepwise and concerted substitution reactions of 4-methoxybenzyl derivatives and the lifetime of the 4-methoxybenzyl carbocation," *Journal of the American Chemical Society*, vol. 112, no. 26, pp. 9507–9512, 1990.

[35] R. Mozingo and K. Folkers, "Hydrogenolysis of aromatic esters to alcohols," *Journal of the American Chemical Society*, vol. 70, no. 1, pp. 229–231, 1948.

[36] A. B. Norman and J. Read, "Optically active diphenylhydroxyethylamines and isohydrobenzoins. VI. The di-o-methoxyphenylhydroxyethylamines and related substances," *Journal of the Chemical Society*, pp. 1120–1123, 1935.

[37] M. Ahmadi, L. Moradi, and M. Sadeghzadeh, "Synthesis of benzamides through direct condensation of carboxylic acids and amines in the presence of diatomite earth@ IL/ZrCl4 under ultrasonic irradiation," *Research on Chemical Intermediates*, vol. 44, no. 12, pp. 7873–7889, 2018.

[38] I. Mohammadpoor-Baltork, H. Reza Memarian, and K. Bahrami, "Efficient and convenient deprotection of thiocarbonyl to carbonyl compounds using 3-carboxypyridinium and 2, 2′-bipyridinium chlorochromates in solution, dry media, and under microwave irradiation," *Monatshefte for Chemie/Chemical Monthly*, vol. 135, no. 4, pp. 411–418, 2004.

[39] W. Phakhodee, C. Duangkamol, S. Wangngae, and M. Pattarawarapan, "Acid anhydrides and the unexpected N, N-diethylamides derived from the reaction of carboxylic acids with Ph3P/I2/Et3N," *Tetrahedron Letters*, vol. 57, no. 3, pp. 325–328, 2016.

[40] H. H. A. M. Hassan, E. M. E. Mansour, A. M. S. Abou Zeid, E. R. El-Helow, A. F. Elhusseiny, and R. Soliman, "Synthesis and biological evaluation of new nanosized aromatic polyamides containing amido- and sulfonamidopyrimidines pendant structures," *Chemistry Central Journal*, vol. 9, no. 1, p. 44, 2015.

[41] J. Němeček, P. Sychra, M. Macháček et al., "Structure-activity relationship studies on 3, 5-dinitrophenyl tetrazoles as antitubercular agents," *European Journal of Medicinal Chemistry*, vol. 130, pp. 419–432, 2017.

[42] H. Wang, K. Lv, X. Li et al., "Design, synthesis and antimycobacterial activity of novel nitrobenzamide derivatives," *Chinese Chemical Letters*, vol. 30, no. 2, pp. 413–416, 2019.

[43] S. Wangngae, C. Duangkamol, M. Pattarawarapan, and W. Phakhodee, "Significance of reagent addition sequence in the amidation of carboxylic acids mediated by PPh3 and I2," *RSC Advances*, vol. 5, no. 33, pp. 25789–25793, 2015.

[44] G. Pérez, C. A. Terraza, D. Coll et al., "Synthesis and characterization of processable fluorinated aromatic poly (benzamide imide) s derived from cycloalkane substituted diamines, and their application in a computationally driven synthesis methodology," *Polymer*, vol. 162, pp. 121–129, 2019.

[45] Clinical and Laboratory Standards Institute, *Reference Method for Broth Dilution Antifungal Susceptibility Testing of Yeasts*, CLSI, Wayne, PA, USA, 2008.

[46] L. R. Peixoto, P. L. Rosalen, G. L. S. Ferreira et al., "Antifungal activity, mode of action and anti-biofilm effects of Laurus nobilis Linnaeus essential oil against *Candida* spp," *Archives of Oral Biology*, vol. 73, pp. 179–185, 2017.

[47] J. Uno, M. L. Shigematsu, and T. Arai, "Primary site of action of ketoconazole on *Candida albicans*," *Antimicrobial Agents and Chemotherapy*, vol. 21, no. 6, pp. 912–918, 1982.

[48] Ł Popiołek, K. Paruch, P. Patrejko, A. Biernasiuk, and M. Wujec, "New 3-hydroxy-2-naphthoic hydrazide derivatives: thiosemicarbazides and 1, 2, 4-triazole-3-thiones, their synthesis and in vitro antimicrobial evaluation," *Journal of the Iranian Chemical Society*, vol. 13, no. 10, pp. 1945–1951, 2016.

[49] Z. N. Siddiqui, F. Farooq, T. M. Musthafa, A. Ahmad, and A. U. Khan, "Synthesis, characterization and antimicrobial evaluation of novel halopyrazole derivatives," *Journal of Saudi Chemical Society*, vol. 17, no. 2, pp. 237–243, 2013.

[50] A. Escalante, M. Gattuso, P. Pérez, and S. Zacchino, "Evidence for the mechanism of action of the antifungal phytolaccoside B isolated from Phytolacca tetramera Hauman," *Journal of Natural Products*, vol. 71, no. 10, pp. 1720–1725, 2008.

[51] I. d A. Freires, R. M. Murata, V. F. Furletti et al., "*Coriandrum sativum* L. (Coriander) essential oil: antifungal activity and mode of action on Candida spp., and molecular targets affected in human whole-genome expression," *PLoS One*, vol. 9, no. 6, Article ID e99086, 2014.

[52] I. O. Lima, F. D. O. Pereira, W. A. D. Oliveira et al., "Antifungal activity and mode of action of carvacrol against *Candida albicans* strains," *Journal of Essential Oil Research*, vol. 25, no. 2, pp. 138–142, 2013.

[53] D. S. Perlin, "Current perspectives on echinocandin class drugs," *Future Microbiology*, vol. 6, no. 4, pp. 441–457, 2011.

[54] C. G. Pierce, A. Srinivasan, P. Uppuluri, A. K. Ramasubramanian, and J. L. López-Ribot, "Antifungal therapy with an emphasis on biofilms," *Current Opinion in Pharmacology*, vol. 13, no. 5, pp. 726–730, 2013.

[55] M. S. Skrzypek, J. Binkley, G. Binkley, S. R. Miyasato, M. Simison, and G. Sherlock, "The Candida Genome Database (CGD): incorporation of Assembly 22, systematic identifiers and visualization of high throughput sequencing data," *Nucleic Acids Research*, vol. 45, no. D1, pp. D592–D596, 2017.

[56] M. J. Keiser, B. L. Roth, B. N. Armbruster, P. Ernsberger, J. J. Irwin, and B. K. Shoichet, "Relating protein pharmacology by ligand chemistry," *Nature Biotechnology*, vol. 25, no. 2, pp. 197–206, 2007.

[57] S. F. Altschul, T. L. Madden, A. A. Schäffer et al., "Gapped BLAST and PSI-BLAST: a new generation of protein database search programs," *Nucleic Acids Research*, vol. 25, no. 17, pp. 3389–3402, 1997.

[58] H. Turkez, F. R. D. Nóbrega, O. Ozdemir et al., "NFBTA: a potent cytotoxic agent against glioblastoma," *Molecules*, vol. 24, no. 13, p. 2411, 2019.

[59] S. P. Lopes, Y. P. Castillo, M. L. Monteiro et al., "Trypanocidal mechanism of action and *in silico* studies of *p*-coumaric acid derivatives," *International Journal of Molecular Sciences*, vol. 20, no. 23, p. 5916, 2019.

[60] Y. Perez-Castillo, T. C. Lima, A. R. Ferreira et al., "Bioactivity and molecular docking studies of derivatives from cinnamic and benzoic acids," *BioMed Research International*, vol. 2020, pp. 1–13, 2020.

[61] P. C. D. Hawkins, A. G. Skillman, G. L. Warren, B. A. Ellingson, and M. T. Stahl, "OpenEye Scientific Software," 1997, https://www.eyesopen.com.

[62] OpenEye Scientific Software, "QUACPAC. Santa Fe, NM: OpenEye scientific software," 2021, http://www.eyesopen.com.

[63] H. M. Berman, J. Westbrook, Z. Feng et al., "The protein Data Bank," *Nucleic Acids Research*, vol. 28, no. 1, pp. 235–242, 2000.

[64] S. Bienert, A. Waterhouse, T. A. de Beer et al., "The SWISS-MODEL Repository-new features and functionality," *Nucleic Acids Research*, vol. 45, no. D1, pp. D313–D319, 2017.

[65] G. Jones, P. Willett, R. C. Glen, A. R. Leach, and R. Taylor, "Development and validation of a genetic algorithm for flexible docking 1 1Edited by F. E. Cohen," *Journal of Molecular Biology*, vol. 267, no. 3, pp. 727–748, 1997.

[66] D. A. Case, I. Y. Ben-Shalom, S. R. Brozell et al., *AMBER 2018*, University of California, San Francisco, CA, USA, 2018.

[67] S. Jo, T. Kim, V. G. Iyer, and W. Im, "CHARMM-GUI: a web-based graphical user interface for CHARMM," *Journal of Computational Chemistry*, vol. 29, no. 11, pp. 1859–1865, 2008.

[68] J. Lee, X. Cheng, J. M. Swails et al., "CHARMM-GUI input generator for NAMD, GROMACS, AMBER, OpenMM, and CHARMM/OpenMM simulations using the CHARMM36 additive force field," *Journal of Chemical Theory and Computation*, vol. 12, no. 1, pp. 405–413, 2016.

[69] B. R. Miller, T. D. McGee, J. M. Swails, N. Homeyer, H. Gohlke, and A. E. Roitberg, "MMPBSA.py: an efficient program for end-state free energy calculations," *Journal of Chemical Theory and Computation*, vol. 8, no. 9, pp. 3314–3321, 2012.

[70] T. C. Lima, A. R. Ferreira, D. F. Silva, E. O. Lima, and D. P. de Sousa, "Antifungal activity of cinnamic acid and benzoic acid esters against Candida albicans strains," *Natural Product Research*, vol. 32, no. 5, pp. 572–575, 2018.

[71] A. J. D. M. Santos Oliveira, R. D. de Castro, H. D. L. F. Pessôa, A. Wadood, and D. P. de Sousa, "Amides derived from vanillic acid: coupling reactions, antimicrobial evaluation, and molecular docking," *BioMed Research International*, vol. 2019, pp. 1–11, 2019.

[72] Y. Perez-Castillo, R. C. Montes, C. R. da Silva et al., "Antifungal activity of N-(4-Halobenzyl)amides against *Candida*

spp. and molecular modeling studies," *International Journal of Molecular Sciences*, vol. 23, no. 1, p. 419, 2021.

[73] D. J. Frost, K. D. Brandt, D. Cugier, and R. Goldman, "A whole-cell *Candida albicans* assay for the detection of inhibitors towards fungal cell wall synthesis and assembly," *Journal of Antibiotics*, vol. 48, no. 4, pp. 306–310, 1995.

[74] E. F. Pettersen, T. D. Goddard, C. C. Huang et al., "UCSF Chimera—a visualization system for exploratory research and analysis," *Journal of Computational Chemistry*, vol. 25, no. 13, pp. 1605–1612, 2004.

[75] P. Shannon, A. Markiel, O. Ozier et al., "Cytoscape: a software environment for integrated models of biomolecular interaction networks," *Genome Research*, vol. 13, no. 11, pp. 2498–2504, 2003.

[76] J. M. Becker, S. J. Kauffman, M. Hauser et al., "Pathway analysis of Candida albicans survival and virulence determinants in a murine infection model," in *Proceedings of the National Academy of Sciences of the United States of America*, vol. 107, no. 51, pp. 22044–22049, 2010.

[77] R. Pasrija, S. Krishnamurthy, T. Prasad, J. F. Ernst, and R. Prasad, "Squalene epoxidase encoded by ERG1 affects morphogenesis and drug susceptibilities of *Candida albicans*," *Journal of Antimicrobial Chemotherapy*, vol. 55, no. 6, pp. 905–913, 2005.

[78] H. Nakayama, K. Ueno, J. Uno et al., "Growth defects resulting from inhibiting ERG20 and RAM2 in *Candida glabrata*," *FEMS Microbiology Letters*, vol. 317, no. 1, pp. 27–33, 2011.

[79] S. Bhattacharya, B. D. Esquivel, and T. C. White, "Overexpression or deletion of ergosterol biosynthesis genes alters doubling time, response to stress agents, and drug susceptibility in *Saccharomyces cerevisiae*," *mBio*, vol. 9, no. 4, 18 pages, 2018.

[80] P. Shah, W. S. Wu, and C. S. Chen, "Systematical analysis of the protein targets of lactoferricin B and histatin-5 using yeast proteome microarrays," *International Journal of Molecular Sciences*, vol. 20, no. 17, p. 4218, 2019.

[81] J. C. Rutherford, Y. S. Bahn, B. van den Berg, J. Heitman, and C. Xue, "Nutrient and stress sensing in pathogenic yeasts," *Frontiers in Microbiology*, vol. 10, p. 442, 2019.

[82] T. R. O'Meara, N. Robbins, and L. E. Cowen, "The Hsp90 chaperone network modulates *Candida* virulence traits," *Trends in Microbiology*, vol. 25, no. 10, pp. 809–819, 2017.

[83] L. Whitesell, N. Robbins, D. S. Huang et al., "Structural basis for species-selective targeting of Hsp90 in a pathogenic fungus," *Nature Communications*, vol. 10, no. 1, p. 402, 2019.

[84] F. Van Hauwenhuyse, A. Fiori, and P. Van Dijck, "Ascorbic acid inhibition of *Candida albicans* Hsp90-mediated morphogenesis occurs via the transcriptional regulator Upc2," *Eukaryotic Cell*, vol. 13, no. 10, pp. 1278–1289, 2014.

[85] A. Daina, O. Michielin, and V. Zoete, "SwissADME: a free web tool to evaluate pharmacokinetics, drug-likeness and medicinal chemistry friendliness of small molecules," *Scientific Reports*, vol. 7, no. 1, Article ID 42717, 2017.

[86] D. E. V. Pires, T. L. Blundell, and D. B. Ascher, "pkCSM: predicting small-molecule pharmacokinetic and toxicity properties using graph-based signatures," *Journal of Medicinal Chemistry*, vol. 58, no. 9, pp. 4066–4072, 2015.